



Optical vegetation indices for monitoring terrestrial ecosystems globally

Yelu Zeng¹, Dalei Hao^{2✉}, Alfredo Huete³, Benjamin Dechant^{4,5}, Joe Berry⁶, Jing M. Chen⁷, Joanna Joiner⁸, Christian Frankenberg^{9,10}, Ben Bond-Lamberty¹⁰, Youngryel Ryu¹², Jingfeng Xiao¹³, Ghassem R. Asrar¹⁴ and Min Chen^{1✉}

Abstract | Vegetation indices (VIs), which describe remotely sensed vegetation properties such as photosynthetic activity and canopy structure, are widely used to study vegetation dynamics across scales. However, VI-based results can vary between indices, sensors, quality control measures, compositing algorithms, and atmospheric and sun–target–sensor geometry corrections. These variations make it difficult to draw robust conclusions about ecosystem change and highlight the need for consistent VI application and verification. In this Technical Review, we summarize the history and ecological applications of VIs and the linkages and inconsistencies between them. VIs have been used since the early 1970s and have evolved rapidly with the emergence of new satellite sensors with more spectral channels, new scientific demands and advances in spectroscopy. When choosing VIs, the spectral sensitivity and features of VIs and their suitability for target application should be considered. During data analyses, steps must be taken to minimize the impact of artefacts, VI results should be verified with in situ data when possible and conclusions should be based on multiple sets of indicators. Next-generation VIs with higher signal-to-noise ratios and fewer artefacts will be possible with new satellite missions and integration with emerging vegetation metrics such as solar-induced chlorophyll fluorescence, providing opportunities for studying terrestrial ecosystems globally.

The launch of Earth observation satellites starting in 1972 ushered in a new era for global observation and study of vegetation¹ (FIG. 1), and led to the development of vegetation indices (VIs). These indices represent vegetation status conditions through simple mathematical combinations or transformations of reflectance in two or more spectral channels, while minimizing the impacts of other contributing factors, such as soil background, the atmosphere and sun–target–sensor geometry^{2–4}. VIs are obtainable at different scales, from the ground with hand-held spectral sensing devices to tower-based and airborne sensors to satellites, and, hence, can provide measurements from fine to coarse resolutions. They are also highly objective, with no or only minimal assumptions of land cover type and canopy structure. As a result, they have been intensively used in local-scale to global-scale studies, and across the Earth and environmental sciences^{5–7}.

Numerous VIs have been developed since the early 1970s (TABLE 1). Many of them can be easily calculated

from publicly available remote-sensing data and are increasingly applied to complex ecological topics, such as vegetation response to long-term climate change^{8–10}, short-term disturbances^{11,12} and extreme climate events¹³. The simplicity of VIs, however, can be deceptive. The subtleties in processing and interpretation of results require experience and theoretical background, and there are many cases of confusion, misinterpretation and controversy related to their use.

In this Technical Review, we describe the rationale, history and key features of VIs. We focus on the most widely used VIs, clarifying and summarizing their usefulness, relationships, inconsistencies, artefacts and limitations. As most VIs are based on reflectance in the optical wavelengths, we mainly focus on the optical VIs. We use the normalized difference vegetation index (NDVI), the enhanced vegetation index (EVI) and the near-infrared reflectance of vegetation (NIRv) as examples, as they are widely used across a variety of global-scale ecological studies and are representative of common features of many VIs.

✉e-mail: dalei.hao@pnnl.gov;
mchen392@wisc.edu

[https://doi.org/10.1038/
s43017-022-00298-5](https://doi.org/10.1038/s43017-022-00298-5)

Key points

- Optical vegetation indices (VIs) derived from space-borne Earth observations are widely used for monitoring terrestrial ecosystems and tracking plant biophysical, biochemical and physiological properties, vegetation dynamics and environmental stresses.
- Sensor and calibration effects, quality assurance and quality control, bidirectional reflectance distribution function, atmospheric and topographic effects, and snow and soil background effects are among important uncertainty sources of VIs.**
- Potential artefacts must be carefully considered to avoid biased interpretations of the underlying ecological processes resulting from the improper use of VIs.
- VIs based on reflectance ratios such as the normalized difference vegetation index can help reduce sensor calibration, bidirectional effects, atmospheric and topographic effects, but could be sensitive to snow and soil background and scale effects.
- Mathematical analysis shows intrinsic similarity among several widely used VIs, including near-infrared reflectance of vegetation, enhanced vegetation index, two-band version of the enhanced vegetation index and difference vegetation index, whereas the ratio-based normalized difference vegetation index behaves differently.
- Identifying key sensitive wavelengths for target application is the first step towards the optimal use of VIs, followed by an understanding of potential uncertainty sources in the specific ecosystem.

The rationale of VIs

The physical foundation of VIs is built on the understanding of complex light–vegetation interactions. Satellite-measured spectral reflectance is a mixed signal of vegetation canopies, their shadows, soils and possibly other components standing on the land surface, and is commonly co-determined by leaf reflectance, background soil reflectance, canopy structure and sun–sensor geometry. The spectral signature of leaf reflectance is well understood (FIG. 2). Leaf reflectance is relatively lower in the visible (VIS) domain (400–700 nm) because of the strong absorption of photosynthetic pigments, particularly in the non-green wavelengths owing to the absorption of chlorophylls; high leaf reflectance in the near infrared band (NIR; 700–1,300 nm) is usually expected owing to spongy mesophyll; and lower leaf

reflectance happens in the shortwave infrared (SWIR; 1,300–2,500 nm) owing to strong water absorption and, to a lesser degree, other leaf biochemical traits, such as lignin, protein and cellulose content. A typical soil reflectance spectrum monotonically increases with wavelength in the optical domain, except for water absorption in the SWIR band. Canopy structure is a key factor affecting the canopy reflectance, because it determines how much of the incoming light is multiply scattered, absorbed and finally escapes from the canopy. Biophysical or structural parameters such as leaf area index (LAI), leaf angle distribution (LAD) and clumping index (CI) are commonly used to characterize canopy structure. The sun–sensor geometry complicates the canopy reflectance observations, largely owing to the fraction of shadows in view as the relative positions of the light source (sun) and the sensor vary. The atmospheric radiative transfer process is another important factor to consider in practice because the canopy-reflected light could be further absorbed and scattered by atmospheric constituents.

To account for these factors, VIs have been developed based on the simple rationale that the spectral signals from the vegetation, and, more specifically, the vegetation characteristics of interest (for example, vegetation biophysical, biochemical and physiological properties), should be enhanced through the use of ratios, differences and/or derivatives between reflectance from different spectral wavelengths or bands (FIG. 3). This enhancement goes along with reducing or (ideally) suppressing background signals from soil and confounding factors related to vegetation characteristics with overlapping spectral features. However, even for a given vegetation characteristic, it is not straightforward to use one single formula that holds under all conditions. This fact, the interest in various vegetation characteristics and the increasing availability of more and narrower spectral bands from satellite sensors are driving the continuing development of VIs.

A brief history of VIs

The history of VI developments goes back to the early 1970s (FIG. 1). These developments are briefly described in this section.

VIs for plant biophysical properties. The first-generation red–NIR ratio-based and difference-based VIs, including the simple ratio (SR), difference vegetation index (DVI) and NDVI^{14–16} were proposed to quantify vegetation growing condition. These VIs were based on live green vegetation absorbing solar radiation in red light to support photosynthesis but reflecting most of the solar energy in NIR to avoid potential damage from overheating¹⁷ (FIG. 1). Refinements have been introduced to minimize the effects of intervening soil background and atmosphere to better isolate the vegetation contributions, especially for sparse vegetation cover^{2,18}. Examples include an orthogonal-transformation-based perpendicular vegetation index (PVI)¹⁹, soil-adjusted vegetation index (SAVI)⁴, transformed soil-adjusted vegetation index (TSAVI)²⁰ and modified soil-adjusted vegetation index (MSAVI)²¹.

Author addresses

¹Department of Forest and Wildlife Ecology, University of Wisconsin-Madison, Madison, WI, USA.

²Atmospheric Sciences and Global Change Division, Pacific Northwest National Laboratory, Richland, WA, USA.

³School of Life Sciences, University of Technology Sydney, Sydney, New South Wales, Australia.

⁴German Centre for Integrative Biodiversity Research (iDiv) Halle-Jena-Leipzig, Leipzig, Germany.

⁵Leipzig University, Leipzig, Germany.

⁶Department of Global Ecology, Carnegie Institution for Science, Stanford, CA, USA.

⁷Department of Geography and Program in Planning, University of Toronto, Toronto, Ontario, Canada.

⁸NASA Goddard Space Flight Center, Greenbelt, MD, USA.

⁹Division of Geological and Planetary Sciences, California Institute of Technology, Pasadena, CA, USA.

¹⁰Jet Propulsion Laboratory, California Institute of Technology, Pasadena, CA, USA.

¹¹Joint Global Change Research Institute, Pacific Northwest National Laboratory, College Park, MD, USA.

¹²Department of Landscape Architecture and Rural Systems Engineering, Seoul National University, Seoul, South Korea.

¹³Earth Systems Research Center, Institute for the Study of Earth, Oceans, and Space, University of New Hampshire, Durham, NH, USA.

¹⁴Universities Space Research Association, Columbia, MD, USA.

Later, the modified simple ratio (MSR)²² was formulated based on the evaluation of several two-band VIs (for example, SR, NDVI and SAVI) for the purpose of improving the linear relationship with biophysical parameters and reducing the sensitivity to measurement noise²². The reduced simple ratio (RSR) index further increased the sensitivity and correlation to LAI, and reduced the effect of background reflectance by taking the canopy closure and understory contribution of open canopies into account by including the SWIR band²³.

The Global Environment Monitoring Index (GEMI) was introduced in 1992 to reduce atmospheric effects²⁴. The launch of MODIS aboard NASA's Terra and Aqua satellites in the early 2000s opened new opportunities for VI developments with more spectral bands in the optical wavelengths. The atmospherically resistant vegetation index (ARVI) and EVI²⁵ were proposed to minimize the atmospheric effects by introducing a blue band, based

on the fact that the blue and red bands suffer from similar atmospheric impacts and, therefore, a proper use of blue band can help cancel the atmosphere influences on the red band^{25,26}. As the atmospheric correction algorithms improved, the blue band became no longer necessary and the two-band version of the enhanced vegetation index (EVI2)²⁷ with no blue band was developed in 2008, achieving similar performance to EVI²⁷. Therefore, unlike EVI, EVI2 can be calculated based on remote-sensing data that do not have the blue band, such as the AVHRR data.

In 2014, the plant phenology index (PPI)²⁸ was derived for estimating plant canopy growth, especially for evergreen forest phenology over high latitudes²⁸. PPI has a nearly linear relationship with green LAI, and soil brightness variations have moderate impact on PPI. Subsequently, NIRv⁵ and the fluorescence correction vegetation index (FCVI)²⁹ were introduced because of

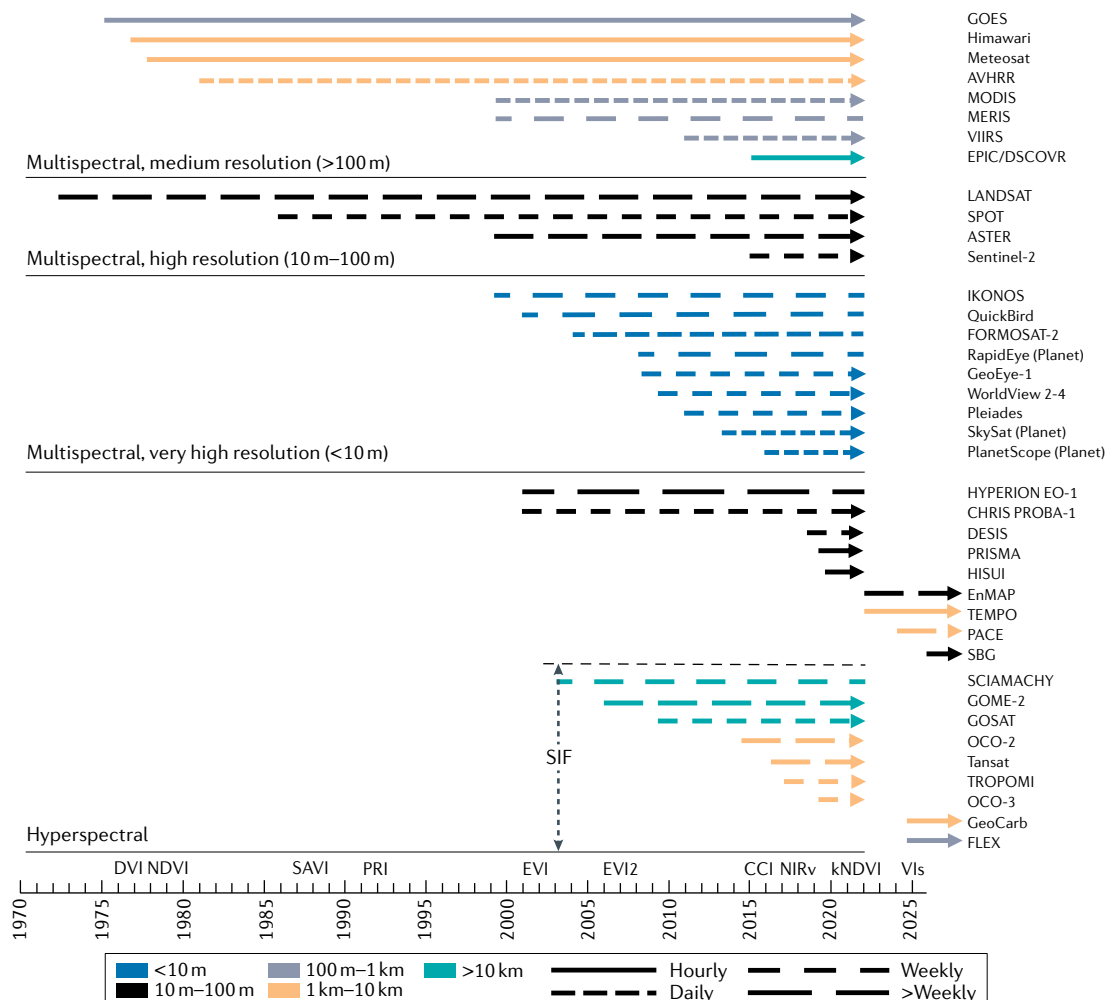


Fig. 1 | Timeline of widely used satellites with the capability to derive vegetation indices. Years active and spatio-temporal resolutions shown for satellites commonly used to derive vegetation indices (VIs). Common VIs are listed above the timeline in the year they were proposed. Many Earth observation satellites have been launched since the early 1970s, continuously providing global observations of terrestrial ecosystems at various spatial, temporal and spectral resolutions. Full definitions of satellite names are in the Supplementary information. CCI, chlorophyll/carotenoid index; DVI, difference vegetation index; EVI, enhanced vegetation index; EVI2, two-band version of the enhanced vegetation index; kNDVI, kernel normalized difference vegetation index; NDVI, normalized difference vegetation index; NIRv, near-infrared reflectance of vegetation; PRI, photochemical reflectance index; SAVI, soil-adjusted vegetation index; SIF, solar-induced chlorophyll fluorescence.

TECHNICAL REVIEWS

Table 1 | Selected widely used optical vegetation indices, spectral ranges and references

Name	Abbreviation	Equation and derivation	Primary applications, advantages and disadvantages
Red-NIR			
Simple ratio ¹⁴	SR	NIR/Red	Structure; simple, but sensitive to the red band atmospheric correction
Normalized difference vegetation index ^{14–16}	NDVI	$\begin{aligned} &(\text{NIR} - \text{Red}) / (\text{NIR} + \text{Red}) \\ &= (\text{SR} - 1) / (\text{SR} + 1) \\ &= 1 - 2 / (\text{SR} + 1) \end{aligned}$	Structure; simple, but sensitive to soil background variations
Modified simple ratio ²²	MSR	$\frac{\text{NIR}/\text{Red} - 1}{\sqrt{\text{NIR}/\text{Red} + 1}}$	Structure; relatively linear relationship with canopy structure parameters, but with small sensitivity to overstory vegetation
Difference vegetation index ¹⁹	DVI	NIR–Red	Structure; simple, but sensitive to the BRDF effect
Perpendicular vegetation index ¹⁹	PVI	$\sqrt{(\text{NIR}_{\text{soil}} - \text{NIR}_{\text{veg}})^2 + (\text{Red}_{\text{soil}} - \text{Red}_{\text{veg}})^2}$	Structure; minimizes soil background influence, but requires the slope and intercept of the soil line
Soil-adjusted vegetation index ⁴	SAVI	$(1 + L) \cdot (\text{NIR} - \text{Red}) / (\text{NIR} + \text{Red} + L)$	Structure; minimizes soil background influence, but sensitive to the BRDF effect
Two-band version of the enhanced vegetation index (EVI) without the blue band ²⁷	EVI2	$2.5 \cdot (\text{NIR} - \text{Red}) / (\text{NIR} + 2.4 \cdot \text{Red} + 1)$	Structure; minimizes soil background influence and no blue band requirement, but sensitive to the BRDF effect
Near-infrared reflectance of vegetation ⁵	NIRv	NDVI · NIR	Structure; minimizes soil background influence, but sensitive to the BRDF effect
Hyperspectral near-infrared reflectance of vegetation ¹⁶⁰	NIRvH	$\text{NIR} - \text{Red} - k(\lambda_{\text{NIR}} - \lambda_{\text{Red}})$	Structure; minimizes soil background influence stronger than NIRv, but sensitive to the BRDF effect
Kernel normalized difference vegetation index ³¹	kNDVI	$\tanh(\text{NDVI}^2)$	Structure; higher sensitivity to canopy structural parameters and GPP
Plant phenology index ²⁸	PPI	$-K \cdot \ln\left(\frac{M - \text{DVI}}{M - \text{DVI}_S}\right)$	Structure; linearly related to green LAI, less severely impacted by snow than NDVI and EVI, and works well for phenology at high latitudes; requires soil DVI
VIS–NIR			
Enhanced vegetation index ²⁵	EVI	$2.5 \cdot (\text{NIR} - \text{Red}) / (\text{NIR} + 6 \cdot \text{Red} - 7.5 \cdot \text{Blue} + 1)$	Structure; minimizes both soil and atmospheric effects, but sensitive to the BRDF effect and requires the blue band
Fluorescence correction vegetation index ²⁹	FCVI	NIR–VIS	Structure; minimizes soil background influence, but sensitive to the BRDF effect
VIS			
Photochemical reflectance index ⁴⁹	PRI	$(\text{R}_{531} - \text{R}_{570}) / (\text{R}_{531} + \text{R}_{570})$	Physiological; tracks the diurnal changes of photosynthetic activity, but complications associated with diurnal sun angle changes must be reduced
Chlorophyll/carotenoid index ⁶	CCI	$\frac{\text{Band}_{11} - \text{Band}_1}{\text{Band}_{11} + \text{Band}_1}$ for MODIS sensor	Physiological and biochemical; tracks the seasonality of daily GPP and phenology for evergreen conifers at multiple spatial scales
Green chromatic coordinate ^{50,189}	GCC	Green/(Red + Green + Blue)	Physiological; structure; biochemical; sensitive to changes in both carotenoid and chlorophyll, correlates well with GPP seasonality but less so to CCI and PRI, and can be easily acquired using RGB imagery
Red-edge NIR			
Red-edge chlorophyll index ³³	Clred-edge	NIR/RE – 1	Biochemical: chlorophyll; linear relationship between the chlorophyll content in maize and soybean leaves with Clred-edge
Red-edge NDVI ³⁴	NDVIRE	$(\text{NIR} - \text{RE}) / (\text{NIR} + \text{RE})$	Biochemical: chlorophyll; directly proportional to chlorophyll and indicates leaf senescence
MERIS total chlorophyll index ³⁵	MTCI	$(\text{R}_{750} - \text{R}_{710}) / (\text{R}_{710} - \text{R}_{680})$	Biochemical: chlorophyll; correlates strongly with red-edge position and is sensitive to high values of chlorophyll content

Table 1 (cont.) | Selected widely used optical vegetation indices, spectral ranges and references

Name	Abbreviation	Equation and derivation	Primary applications, advantages and disadvantages
NIR–SWIR			
Normalized difference water index ⁴²	NDWI	$\frac{\text{NIR}_{860} - \text{SWIR}_{1240}}{\text{NIR}_{860} + \text{SWIR}_{1240}}$	Biochemical: water content; sensitive to vegetation water content changes, less sensitive to atmospheric effects than NDVI, but does not completely remove the soil background reflectance effect
SWIR			
Normalized difference lignin index ⁴⁷	NDLI	$[\log(1/R_{1754}) - \log(1/R_{1680})]/[\log(1/R_{1754}) + \log(1/R_{1680})]$	Biochemical: lignin; significantly correlates to foliar lignin concentration in green canopies, but unable to assess foliar or bulk canopy lignin in senescent vegetation
Cellulose absorption index ¹⁹⁰	CAI	$100 \cdot [0.5 \cdot (R_{2019} + R_{2206}) - R_{2109}]$	Biochemical: cellulose; positive for all crop residues, while all soils have negative values, and, thus, can discriminate crop residues from soil under dry and moist conditions
VIS–NIR–SWIR			
Reduced simple ratio ²³	RSR	$\text{SR} \cdot \left(1 - \frac{\text{SWIR} - \text{SWIR}_{\min}}{\text{SWIR}_{\max} - \text{SWIR}_{\min}}\right)$	Structure; increased sensitivity and correlation to LAI than SR in boreal forests, and reduced the effect of background reflectance

Subheadings represent spectral range. For a more comprehensive list of vegetation indices, see Supplementary Table 1. BRDF, bidirectional reflectance distribution function; GPP, gross primary production; LAI, leaf area index; NIR, near infrared; SWIR, shortwave infrared; VIS, visible domain.

their ability to reduce soil background effects on the NIR reflectance of vegetation and to better approximate the vegetation's solar radiation absorption and photosynthesis^{5,30}. NIRv has received substantial attention and widespread application because of its clear physical foundation and strong correlation with vegetation photosynthesis^{5,30} (FIG. 3). In 2021, the kernel normalized difference vegetation index (kNDVI) was proposed based on the theory of kernel methods as a unifying VI for monitoring the terrestrial carbon dynamics and increasing the sensitivity of NDVI to plant biophysical parameters³¹.

VI_s for plant biochemical properties. Broad-band reflectance smooths the detailed spectral signatures, and therefore, the broad-band VIs described in the previous section are primarily designed for detecting vegetation structure and its changes. In parallel, a group of VIs was developed by taking advantage of narrow-band sensor measurements, which keep more detailed spectral information. These narrow-band VIs are specifically designed to describe the biochemical and physiological properties, such as pigments, water, plant residues and nitrogen³², and typically use a combination of strong-absorbing VIS bands and a narrow band located in the red-edge region (670–780 nm). Examples include red-edge chlorophyll index (CIred-edge)³³, red-edge normalized difference vegetation index (NDVIRE)³⁴ and MERIS total chlorophyll index (MTCI)³⁵ for indicating chlorophyll content, the structure insensitive pigment index (SIP)³⁶, normalized pigment chlorophyll ratio index (NPCI)³⁷ and plant senescence reflectance index (PSRI)³⁸ for carotenoid content, and anthocyanin reflectance index (ARI)³⁹, anthocyanin content index (ACI)⁴⁰ and red/green ratio index (RGRI)⁴¹ for anthocyanin content. Using the water absorption bands around 970, 1,200, 1,450, 1,940 and 2,500 nm, normalized difference water index (NDWI)⁴², land surface water index (LSWI)^{43,44} and normalized

difference infrared index (NDII)⁴⁵ were designed with a similar formula and exhibit similarly robust performance on indicating vegetation hydrological condition⁴⁶. The normalized difference lignin index (NDLI) was designed with the 1,754-nm lignin absorption feature and the normalized difference nitrogen index (NDNI) considered the 1,510-nm nitrogen absorption feature⁴⁷.

VI_s for plant physiological properties. Another group of VIs was proposed as indicators of photosynthetic light-use efficiency (LUE) or environmental stresses by detecting stress-induced physiological changes in xanthophyll cycle pigments⁴⁸. Because the reflectance at 531 nm is sensitive to carotenoid pigments and the xanthophyll cycle, the photochemical reflectance index (PRI) with a reference wavelength at 570 nm was put forward in 1992 to track changes in diurnal photosynthetic efficiency⁴⁹. The chlorophyll/carotenoid index (CCI) presented in 2016 is another index for representing the dynamics of the chlorophyll/carotenoid ratio. CCI has the potential to track seasonal variations of canopy photosynthesis at the global scale⁶, because it could be directly obtained from existing satellite data. PRI, CCI and green chromatic coordinate (GCC) can capture the seasonal variation of carotenoid and xanthophyll cycles over temperate evergreen needleleaf forests that are difficult to detect with broadband VIs such as NDVI and NIRv^{50,51}. Red-edge vegetation stress index (RVSI)⁵² had less negative values for stressed leaves than healthy leaves in grapevine leafroll disease detection over two wine grape cultivars⁵³.

Satellite sensors for VIs. VIs rely on reflectance measurements by a series of Earth observation satellite sensors¹ (FIG. 1) and their use has evolved with the changes in technology. Landsat 1–3 MultiSpectral Scanner (MSS), launched starting in 1972, only had four VIS–NIR bands with about 80-m spatial resolution and a half-monthly revisit cycle. Since Landsat 4 was launched in 1982, the

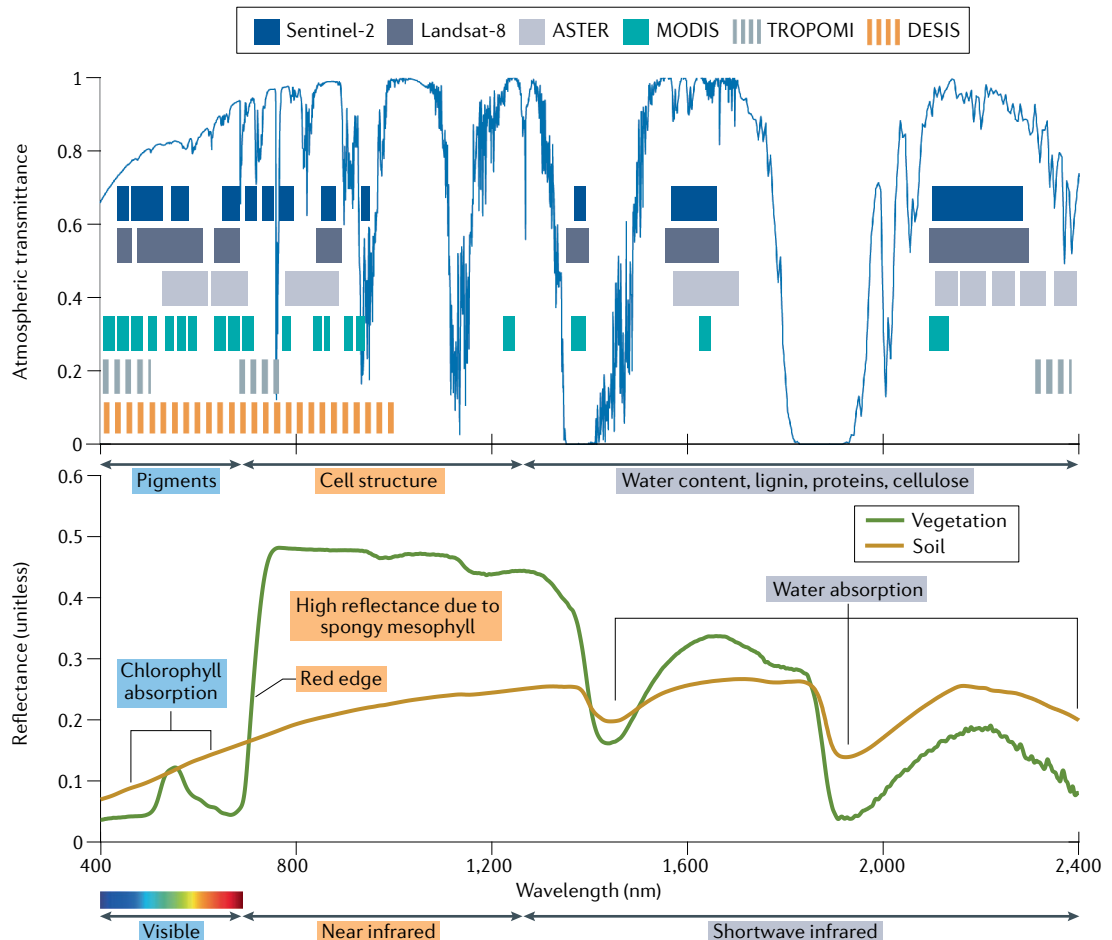


Fig. 2 | Satellite sensors, the vegetation and the soil spectrum across wavelengths. Top: the spectral response range in the atmospheric window of a few widely used satellites¹⁰⁹. The coloured blocks and vertical lines illustrate the spectral band range or bandpass for each satellite sensor. Bottom: reflectance of vegetation and soil. These spectral features of vegetation and soil are the foundation of the rationale of vegetation indices and support the design of various vegetation indices.

spatial resolution in VIS–NIR bands has increased to 30 m. Sensors with similar spatial resolution include SPOT (1986–) and Sentinel-2 (2015–), which have weekly to daily temporal resolution. Sentinel-2 is one of the few sensors with the capability to calculate red-edge VIs for plant pigments. AVHRR, MODIS and VIIRS, launched in 1981, 1999 and 2011, respectively, have daily temporal coverage, while AVHRR does not have the blue band for EVI.

To reach high temporal resolution, geostationary satellites, such as GOES and Himawari, both launched in the 1970s, had sub-hourly VI observations. NDVI, SR and RSR have been employed to generate global LAI products from Himawari, AVHRR and MODIS observations with biome-specific LAI–VI relationship^{54–56}. Global leaf chlorophyll content was first generated from MERIS observations by physically based radiative transfer models instead of the chlorophyll-sensitive MTCI, due to the impact of LAI on MTCI⁵⁷. For very high spatial resolution (<10 m), GeoEye-1, WorldView 2–4, Pleiades, SkySat and PlanetScope have been available since 2009 but can only provide VIS–NIR reflectance for vegetation biophysical properties. DESIS and HISUI on the International Space Station, as well as Hyperion and

PRISMA, provide hyperspectral observations. However, they only have an approximately monthly revisit cycle, which is suitable for plant biochemical and physiological traits mapping but not capturing rapid temporal changes of vegetation.

Ecological applications of VIs

VIs have been successfully applied to ecological research ranging from monitoring vegetation changes to investigating vegetation feedbacks to the larger climate system. Some examples are described in this section^{58–60}.

Estimating vegetation attributes. VIs are widely used to estimate biophysical essential climate variables such as LAI, fraction of absorbed photosynthetically active radiation (FPAR) and above-ground biomass^{54,55,61}. They are often used as a direct proxy of the target variables^{62–64}, but can also be used to calculate these variables, which are then used in further analysis. For example, NDVI and EVI have been commonly used as proxies for FPAR^{54,55} and NDVI has been used as a robust indicator of LAI and fractional vegetation cover⁶⁵. However, NDVI has a few well-known drawbacks, such as its insensitivity to densely vegetated areas and the oversensitivity to the

changes of soil brightness due to rainfall and snowfall. As the saturation point of EVI is higher than that of NDVI^{25,27}, EVI is often used in densely vegetated areas such as tropical forests. Chlorophyll-corrected VIs in particular can minimize the impact of chlorophyll content on LAI estimations. For example, a modified triangular vegetation index (MTVI2) and a modified chlorophyll absorption ratio index (MCARI2) were the best predictors of green LAI in a systematic evaluation of more than ten VIs (including NDVI, MSR and SAVI) over various crops⁶⁶.

Red-edge VIs have been widely used for estimating leaf and canopy chlorophyll content and carotenoid

pigments⁶⁷, whereas SWIR-based VIs were often roughly used for estimating leaf and canopy water content, leaf mass per area (LMA) and nitrogen content³² (TABLE 1). These retrieved plant traits can be directly used to quantify the functional diversity. The spatial distribution and textural feature of VIs such as MODIS EVI were also used to study spectral diversity, species richness and habitat heterogeneity^{68,69}.

Temporal vegetation dynamics. NDVI and EVI are the most widely used VIs for detecting and monitoring temporal vegetation dynamics because of their simplicity, robustness and availability, especially for tracking

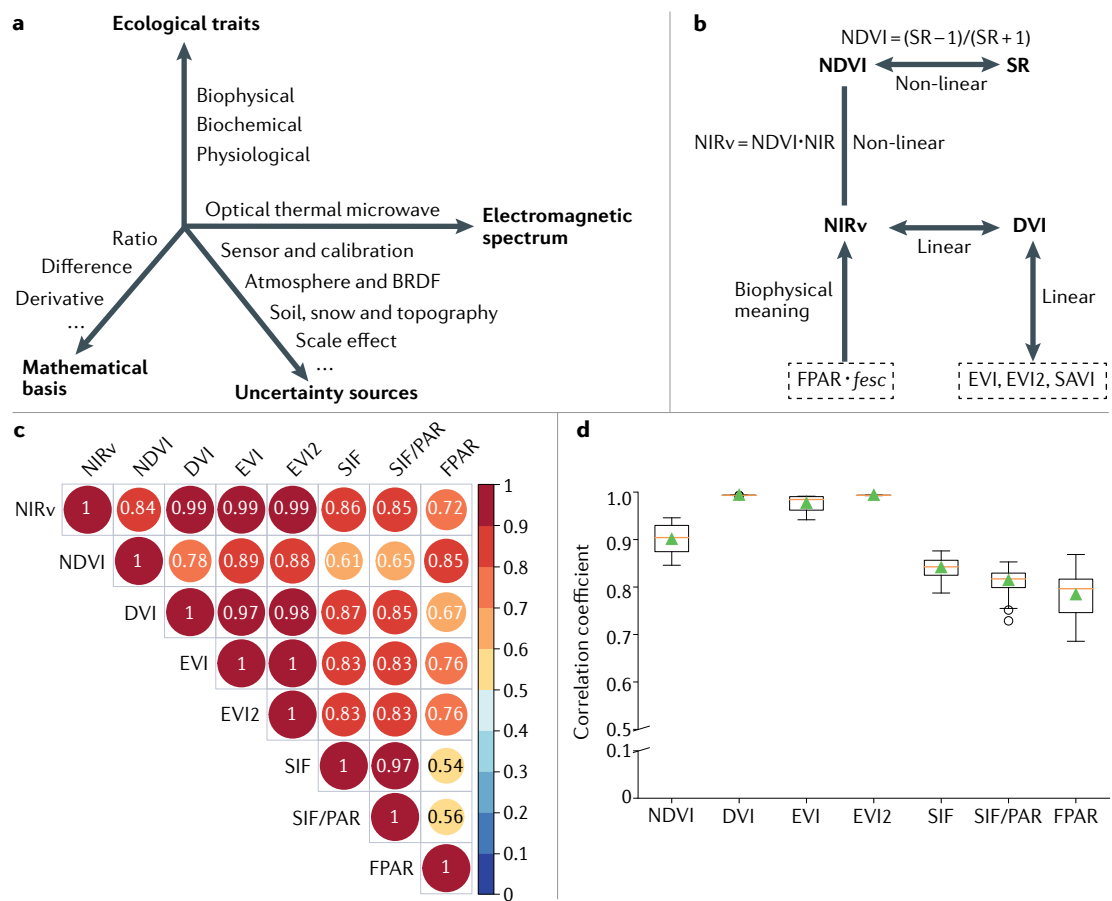


Fig. 3 | The taxonomy, physical meaning and similarity of vegetation indices. Vegetation indices (VIs) are developed with different spectral bands and mathematical formulae, used for indicating different ecological traits and suffer varied artefacts, while several of the most widely used VIs have intrinsic similarities. **a |** The taxonomy of VIs from four different dimensions: physics, mathematics, ecology and uncertainties. **b |** The biophysical interpretation and intrinsic linkage of several widely used VIs. **c |** Global spatial correlations of monthly averaged MODIS near-infrared reflectance of vegetation (NIRv), normalized difference vegetation index (NDVI), difference vegetation index (DVI), enhanced vegetation index (EVI), two-band version of the enhanced vegetation index (EVI2), solar-induced chlorophyll fluorescence (SIF), photosynthetically active radiation (PAR)-normalized solar-induced chlorophyll fluorescence (SIF/PAR) and fraction of absorbed photosynthetically active radiation (FPAR) in August 2018 and at 0.1° spatial resolution, considered as the peak growing month for most vegetation types. The size of the circle corresponds to the correlation. In the spatial aggregation, the red, near infrared (NIR) and blue reflectance was first averagely aggregated to 0.1° and then the VIs were calculated. **d |** Global spatial correlations between MODIS NIRv and other remote-sensing VIs during March 2018–February 2019 since the origin of TROPOMI SIF, with the temporal resolution of 4 days and 0.1° spatial resolution. In the box plot, green triangles refer to the mean value, boxes represent the interquartile ranges of the 25th (Q25) and 75th (Q75) percentiles, and whiskers cover the ranges of $Q25 - 1.5 \cdot (Q75 - Q25)$ and $Q75 + 1.5 \cdot (Q75 - Q25)$. The R between NIRv and other VIs ranged from 0.78 to 0.89. NDVI has a relatively larger R with FPAR, but has a weaker linear correlation with SIF than the other VIs. BRDF, bidirectional reflectance distribution function; fesc, photon escape probability from the canopy; SAVI, soil-adjusted vegetation index; SR, simple ratio.

seasonal changes (phenology) and long-term trends of structural changes^{8,70–72}. Indeed, EVI and EVI2 are the primary data source for producing the MODIS vegetation phenology product Collections 5 and 6, respectively^{7,74}. However, NIRv has been gaining popularity for vegetation change analyses using ecosystem gross primary production (GPP)⁷⁵. Moreover, PPI and EVI2 performed better than NDVI with Sentinel-2 imagery across Europe when compared with ground-observed phenological stages, especially for evergreen coniferous forest during winter with snow⁷⁶. CCI better tracked evergreen forest phenology and the end-of-season changes in deciduous forests than structurally oriented NDVI, EVI and NIRv⁷⁷. These examples demonstrate the need to consider the inter-sensor consistency and the sun-sensor geometry, and the community awareness that VIs are subject to such artefacts at different levels of sensitivity.

Environmental stresses and disturbances. The abrupt temporal changes of VI time series are useful for the detection of land cover change, environmental stress and disturbance. EVI has been widely used to monitor and quantify the deforestation and degradation in the Amazon tropical rainforest⁷⁸, and the responses to drought, heatwave and water stresses^{11,12,79}. Using PRI, CCI and GCC describes stronger seasonal physiological changes of vegetation than using structurally oriented VIs such as NDVI and EVI in dormant temperate forests^{50,51}. Biochemically related VIs such as SIPI, NPCI and ARI have also been applied for the detection of pests and diseases in winter wheat⁸⁰ and soil erosion and heavy metal pollution in rice paddies⁸¹, especially when hyperspectral data are available. Forecasting wildfire risks, monitoring fire severity and characterizing vegetation recovery after fire disturbance can be typically achieved by simple VIs such as NDVI, while hyperspectral imaging spectroscopy and light detection and ranging (LiDAR) are encouraged to be used in combination for the assessment of fuel condition and vegetation structure mapping¹³. NDVI has also been used for the assessment of ecosystem integrity and land degradation and desertification at different scales, including the resilience of agroecosystems⁸².

Ecosystem carbon and water fluxes. Vegetation dynamics drive changes in the surface radiation regime, which co-determine microclimate and land–atmosphere carbon and water fluxes, as tracked using VIs as a proxy for vegetation canopy coverage, LAI and FPAR (FIG. 3). FPAR is usually considered a function of LAI and, thus, the advantages and disadvantages of the VIs for monitoring LAI also apply to the carbon and water flux estimations. Some notable examples of using VIs to estimate carbon fluxes, particularly GPP, include the Carnegie–Ames–Stanford approach (CASA)⁸³, MODIS algorithm⁸⁴ and EC-LUE model⁸⁵ (all using NDVI-derived FPAR); vegetation photosynthesis model (VPM)⁴⁴, the modified GPP model in TEM⁸⁶, data-driven GPP upscaling⁸⁷ (using EVI); simpler statistical upscaling using NIRv^{30,88}, regional forest GPP estimations⁸⁹ (using EVI2); satellite-based GPP with implicit parameterization of LUE^{7,88} (using NDVI and

soil-adjusted NIRv, SANIRv). All these approaches have moderate to high success. NIRv in particular has received growing attention because of its explicit physical link to FPAR^{30,90,91} and moderate relationship with LUE⁹². PRI, CCI and GCC are also used to track the seasonal GPP dynamics, although it is still challenging to establish quantitative relationships between these VIs and LUE for robust GPP estimations. Nevertheless, the inclusion of PRI together with NDVI had shown improvements in estimating boreal forest CO₂ fluxes⁹³.

VIs have been used as direct indicators of photosynthesis, such as when examining CO₂ fertilization effects by using AVHRR and MODIS NIRv^{63,94}, carbon loss in Amazon rainforest degradation and deforestation with MODIS EVI⁷⁸, the change velocity and optimum air temperature of productivity across biomes by MODIS NDVI and NIRv⁶², and the anomalies and recovery of tropical forest during the strong 2015/2016 El Niño event, along with MODIS EVI⁹⁵. Estimating below-ground carbon fluxes from satellite observations has rarely been attempted and is based on indirect correlations between GPP and soil respiration via VIs⁹⁶. Typically, NDVI, EVI and MSAVI are used as scaling factors to extrapolate field-level soil respiration measurements to larger scales^{96,97}.

Another prominent, long-standing application of VIs is estimating evapotranspiration (ET)^{98,99}. VIs are powerful indicators of the fraction of vegetation coverage, absorption of solar energy and canopy roughness, which are major determinants of ET^{100,101}. As a result, even though ET is more accurately assessed using land surface temperature (LST), VIs can be used to estimate ET and are more readily available. Moreover, owing to the strong VI–LST or VI–ET correlations observed at the flux tower sites, VIs are used to upscale site observations and enhance or downscale satellite LST, especially when LST data are unavailable or have a coarse resolution^{100,102}. NDVI, SAVI and EVI are, so far, the most widely used VIs in a variety of ET estimation models^{101–103}. However, owing to the sensitivity of NDVI to soil brightness, the more soil-resistant VIs, such as EVI, EVI2, NIRv and SAVI, are considered better choices^{98,100,102}. Used as a direct or indirect proxy of ET, VIs can be further applied to investigate vegetation feedbacks to the climate system. For example, NDVI has been used to analyse the climatic effects of vegetation growth, suggesting strong regional and global coupling between vegetation and LST and precipitation^{104–106}.

Artefacts that cause inconsistencies

Inconsistencies in VI-based results are common, in part owing to the use of different VIs and in part related to artefacts of VI products derived from different sensors (Supplementary Table 2), satellite product versions, atmospheric and directional corrections, compositing algorithms and the application of different levels of quality assurance (QA) and quality control (QC) flags⁷⁹. A comprehensive understanding of these inconsistencies and the limitations and caveats of each VI is essential to the rigorous use of VIs and the correct interpretation of the results. This section discusses these artefacts and their impacts on analyses (FIG. 4).

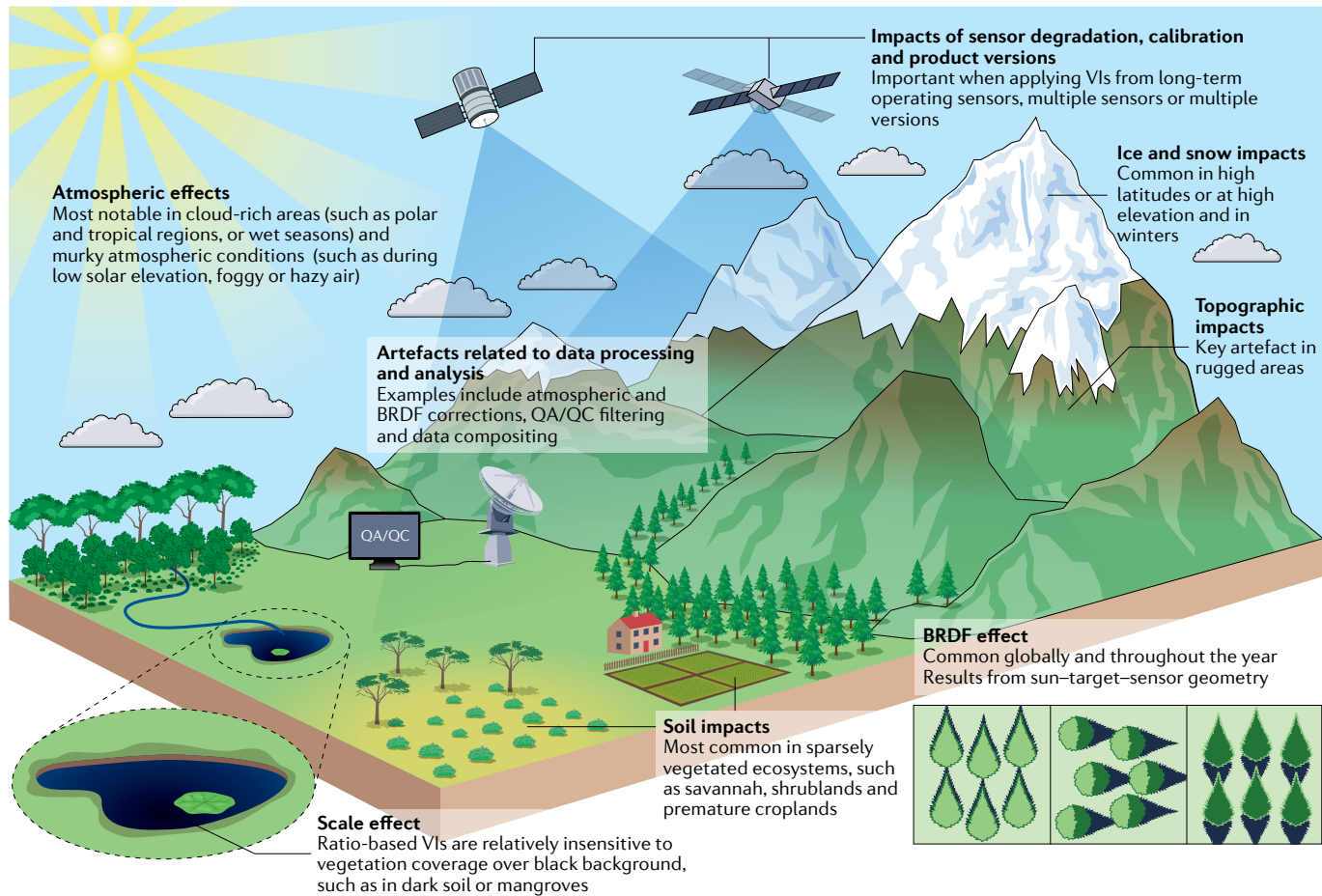


Fig. 4 | Vegetation indices artefacts and uncertainties. Uncertainties come from different sensors, calibration, quality control (QC) flags, compositing algorithms, the atmosphere, bidirectional reflectance distribution function (BRDF) effects, soil and snow background, topography and scale effects. Potential uncertainties can vary with ecosystems, latitudes, atmospheric conditions and surface landscapes. QA, quality assurance; VIs, vegetation indices.

Sensor and calibration effects. There can be inconsistencies in different satellite time series within the same study area as a result of sensor and calibration effects. For example, vegetation greenness trends derived from AVHRR versus MODIS NDVI time series apparently show trends in opposing directions¹⁰⁷. The differences in the central wavelength and range of the spectral response function between sensors can be important contributing factors for such inconsistencies^{108,109}. For example, NDVI obtained from AVHRR, MODIS and VIIRS shows substantial differences in values, and the level of the differences varies across land cover types, although their orbits and spatio-temporal resolutions are similar¹⁰.

Besides intrinsic differences between technologies, satellites and their sensors often suffer from the harsh space environment, resulting in orbital drift and sensor degradation over time. Although on-board calibration or vicarious calibration is applied to maintain the measuring standards, the remaining limitations can affect the accuracy of the derived VIs and introduce systematic biases, especially in long-term trend analyses^{110,111}. Products from AVHRR and MODIS are typical examples of this phenomenon^{112,113}. AVHRR measurements come from a series of satellites, each of which has specific

orbital characteristics^{114,115} that can affect the image acquisition time and sun-target-sensor geometry¹¹³. In particular, NDVI values from AVHRR aboard NOAA-11 were markedly higher than those from prior and subsequent AVHRR sensors¹¹⁶.

Orbital drift effects were also found in the VIP3 and LTD4 NDVI data and over the more humid areas for GIMMS-3g NDVI. Indeed, a study using AVHRR NIRv as a long-term consistent record found that the trend in CO₂ fertilization effects on global vegetation photosynthesis declined in most of the regions from 1982 to 2015 (REF.⁶³). However, concerns were raised about potential uncertainties in the conclusion partly due to sensor differences^{114,113}. MODIS-based NDVI exhibited an increasing trend during 2001–2016, while a decreasing trend of the GIMMS-based NDVI was observed, especially after 2012, suggesting large discrepancies in global greening¹¹⁷. As another example, an abrupt positive jump in the SPOT-VGT NDVI time series was identified owing to the platform and sensor change from VGT-1 to VGT-2 (REF.⁹).

Another important issue is that different VIs can show varying sensitivity to sensor calibration owing to their mathematical formulae. The calibration bias can affect both VIS and NIR bands similarly, and, thus, at least partly

cancel out in ratio-based VIs such as NDVI and SR¹¹⁸. For example, the single-band reflectance calibration uncertainty for MODIS was 2% under normal atmosphere conditions, whereas the mean NDVI uncertainty due to sensor calibration was only ± 0.01 units and was less than 2% of the dynamic range using field canopy reflectance observations¹¹⁸. The cross-sensor difference in NDVI could also be smaller than the difference in surface reflectance. In a comparison between 15 moderate-resolution sensors including MODIS, VIIRS and AVHRR, each pair of sensors had a larger coefficient of determination (R^2) and smaller root-mean-square error (RMSE) for NDVI than for the VIS and NIR bands separately¹⁰.

In VIs such as NIRv (=NDVI \times NIR), such calibration biases do not cancel out, impacting the absolute values of the VI signals as NIR reflectance is multiplied. Although this could be problematic for applications that rely on the absolute values of VI, it could also be an issue for the consistency of long-term time series when there are differences in calibration bias between different sensors or calibration drift of a given sensor over time. Therefore, differences in vegetation trends and magnitudes for different VIs can be due to both the inherent characteristics of the VIs and their different sensitivities to calibration bias.

Product versions. VI satellite products are usually produced in different versions (collections) with varying algorithmic improvements and calibration adjustments. Using different VI product versions could lead to inconsistent interpretation of changes in the vegetation. For example, there are inconsistent greening or browning trends between MODIS Collection 5 (C5) and Collection 6 (C6) products¹¹¹. MODIS itself suffers from sensor degradation, which is larger for the Terra satellite, especially in the blue band^{111,119}. The degree of degradation decreases with increasing wavelength, and, thus, there are negative decadal trend artefacts for MODIS Terra products with $\Delta\text{NDVI} \approx 0.01$ and $\Delta\text{EVI} \approx 0.02$ (REF.¹¹⁹) when comparing C5 with an enhanced C6 (C6+) version. The percentage of negative MODIS-C5 NDVI trends derived from Terra (17.4%) was nearly three times as large as that derived from Aqua (6.7%) for North America during 2002–2010 (REF.¹¹⁰). Most of the vegetation browning trends revealed by MODIS Terra-C5 VIs were likely caused by sensor degradation, particularly during the period after 2007, so previous studies of vegetation trends based on only Terra-C5 VIs might need to be re-evaluated¹¹¹. The latest MODIS C6 has sensor degradation corrected and better consistency between Terra and Aqua measurements, and provides a more reliable record than C5 (REF.¹¹⁹).

Pre-processing steps. Standard VI products usually include important data pre-processing and sensor configuration information, such as the sun-target-sensor geometry and QA/QC, which could introduce critical errors in the subsequent analyses if not taken into account appropriately. The relative positions of the sun, sensor and observing target commonly change over time owing to the continuous movement of Earth, sun and satellites. Such changes result in variations in solar

illumination and sensor viewing angles, and strongly affect remotely sensed observations^{64,120,121}. This effect can be mathematically described as the bidirectional reflectance distribution function (BRDF) effect or the sun-target-sensor geometry effect (FIG. 4).

The solar angle varies seasonally and latitudinally but is annually repetitive if a sensor remains in a stable orbit. Therefore, the variations can influence VI-based phenology measurements but not the long-term trends or interannual variations. For example, Amazon forests have been reported to exhibit no variations in EVI from wet to dry season, and dry season greening has been attributed to seasonal solar-angle variations⁶⁴. Subsequent studies using either the same data¹²² or the rigorously BRDF-corrected MAIAC product¹²³ suggested dry-season greening but with smaller magnitude, which demonstrates the importance of disentangling solar-angle-induced seasonal variations in VIs from vegetation-induced variations.

Similarly, the BRDF effect drives the satellite NDVI phenology in evergreen sparse canopy ecosystems in western USA with subtle growth dynamics¹²⁴, not the vegetation response. MODIS, Landsat 7, Sentinel-2, VIIRS and Proba-V confirmed this effect with the ground-based PhenoCam observations as the reference. Landsat, which only acquires images at $\pm 7.5^\circ$ from nadir, has relatively small view-angle effects¹²⁵. By contrast, other satellite sensors such as AVHRR and MODIS usually extend to larger view angles, introducing uncertainties to the downstream products if uncorrected^{120,121}. Given the potential impact of solar-angle variation, the VI-based analyses should either be restricted to selected data with consistent sun-target-sensor geometry or the BRDF effect needs to be rigorously removed in the data¹²⁴.

A related uncertainty source is the compositing approach, which determines how to extract the highest-quality observations over the typically used 8-day, 16-day or monthly interval. Compositing has gone through major changes since the introduction of the traditional maximum value compositing (MVC) algorithm, which is still employed in GIMMS-3g datasets. The modified constrained view-angle MVC, or CV-MVC²⁵, is used in MODIS VI compositing (MOD13A1 and MYD13A1), and later the 16-day rolling compositing based on BRDF retrievals was used in MCD43A4 nadir BRDF-adjusted reflectance (NBAR)-VIs¹²⁶. The MOD13A1 and MYD13A1 products with the CV-MVC algorithm aimed to reduce the BRDF effect but still did not theoretically normalize it¹²⁷. The MCD43A4 C6 product removed the view-angle effects but was set at the local solar noon zenith angle¹²⁸, which varies seasonally and latitudinally. Compositing approaches vary widely and can lead to inconsistent interpretation of results. For example, in the studies conducted over the Amazon^{70,79,129} and the western USA¹²⁴, selective compositing settings based on study objectives resulted in inconsistent results. The MODIS Collection 4 EVI indicated Amazon forest green-up during the 2005 drought¹²⁹, whereas the Collection 5 data with improved input-data filtering did not support this phenomenon⁷⁹. In the western USA, the extent of the NDVI peak in winters could vary owing to temporal compositing¹²⁴.

Another source of inconsistency is the atmospheric correction, which has been conducted fully, partially or sometimes not at all for different VI products. MODIS attempted the full correction, while GIMMS had limited correction. NDVI derived from VIIRS observations is based on top-of-atmosphere reflectance, whereas VIIRS EVI is generated based on surface reflectance¹³⁰. Even when calculated from atmospherically corrected reflectance at the surface, VIs are still subject to uncertainties in atmospheric correction, such as cloud masking, residual sub-pixel clouds, incomplete corrections for Rayleigh scattering, ozone, water vapour absorptions and imperfect aerosol correction¹³¹. For example, in the studies on the impact of drought on Amazon forests, where VIs were intensively used, large differences were found in the extent of Amazon greening during the 2005 drought. These differences were attributed to inadequate QA/QC screening for cloud and aerosol effects⁷⁹.

Soil, snow and topographic effects. Most of Earth's terrestrial ecosystems have sparse canopies with appreciable canopy background signals (such as from soil, litter, snow and water) that can affect satellite-derived VIs. Soil types and soil moisture conditions lead to spatio-temporal variations in soil brightness¹³². In natural ecosystems, the soil layer could be mixed with litter, moss, lichen or waterbodies; woody stems and branches could contribute to the background noise or bias of VIs in forest ecosystems¹³³. Soil influences are assumed to vary the most in arid regions and have the greatest effect in moderately vegetated canopies ($LAI \approx 1$ or $\sim 50\%$ cover). For example, in northern Africa, extensive soil artefacts in the AVHRR-NDVI signals are seen over reddish soils¹³⁴, and in the Sahel, the NDVI variations were reported to be due to soil type, moisture and reflectance differences¹³⁵. The first rains can result in an artefact NDVI flush prior to the actual greening cycle, and similar NDVI soil artefacts can be seen in over-irrigated and freshly ploughed croplands¹³⁶. Snow and ice with high optical reflectance are among the most important factors that lead to the inconsistency of the VI time series during winter in temperate regions^{124,137} or, more permanently, in the Arctic¹³⁸. There is evidence of bias in detecting vegetation phenology phase using NDVI at the end of the non-growing season, owing to the presence of snow, which causes low NDVI values¹³⁹.

Topography, which can cast macroscale shadows and change the local sun–surface–sensor geometry, also impacts surface reflectance¹⁴⁰ and VIs¹⁴¹. Similar to the shadows in view caused by the sun–target–sensor geometry, a topographic shadow is much darker in the red wavelength than in the highly scattered NIR wavelength owing to the multiple scattering between slopes¹⁴². Compared with the sun–target–sensor geometry-induced porous and fuzzy canopy shadows, the dark and opaque topographic shadows can have larger effects on EVI¹⁴¹. The topographic effects on reflectance should be minimized before EVI and other VIs without a band-ratio format (such as NIRv and SAVI) are calculated; the topographic effects on the ratio-based VIs such as SR and NDVI are usually smaller¹⁴¹. The topographic effects are also related to the

spatial scale, so as the size of the pixel increases, the topographic effects can decrease and even disappear with spatial averaging¹⁴³.

Scale-mismatch effects. Spatial mismatches between the region of interest and the predefined grid cells in remote-sensing datasets could be another important source of uncertainty¹⁴⁴. For example, MODIS pixels have accurate geolocation, yet the offset is up to half a pixel between scenes on average, which is significant when users rely on single-pixel VIs to match in situ measurements¹⁴⁵. Considering that the in situ measurement is rarely near the centre of a pixel, there is high probability that a single MODIS pixel might not always sample the in situ measurement area. The sensor point spread function could further distort the matching of gridded satellite data with ground-based data¹⁴⁴. The emerging high-spatial-resolution data (for example, PlanetScope and airborne data, ≤ 3 m) could also lead to difficulties in interpretation. For example, a pixel could be entirely in the shadows of a tree, so that VI values could be highly distorted owing to the lower illumination than the sunlit crown side if the research target is the whole tree canopy¹⁴⁶. Identifying a suitable remote-sensing product at an appropriate spatial scale could be the most effective choice for minimizing such uncertainties.

There is a general lack of studies that use long-term, well-coordinated in situ networks to measure reflected radiation from vegetation to confirm larger-scale greening and browning results. The MODIS EVI results related to the Amazon dry season greening were confirmed with in situ measurements of GPP from eddy covariance flux towers¹⁴⁷. By contrast, the greening trends in the Sahel challenge the mainstream paradigm of irreversible ground-observed land degradation in this region¹⁴⁸.

There is also a debate about whether the onset of spring phenology has been advancing owing to climate warming. The trends in the start of the growing season (SOS) for Tibetan alpine meadow and steppe were examined using ground-based phenology observations and NDVI datasets from GIMMS and GIMMS-3g, MODIS, SPOT-VEG and SeaWiFS¹⁴⁹. There were large discrepancies in the SOS trends between the ground-based and different NDVI datasets, and between the different phenology retrieval, potentially due to NDVI data quality and scale mismatch between satellite and ground data. Similar results were reported by comparing ground-based PhenoCam data with EVI derived from a variety of sensors, including Landsat ETM+, MODIS and DSCOVR-EPIC⁷². At three rural sites and one urban site of deciduous trees in Ireland, AVHRR and MODIS EVI2-derived SOS during 1982–2016 was consistently earlier than in situ leaf unfolding across all these sites, with a RMSE of 25–52 days and mean bias error of –5 to –50 days, whereas satellite-derived growing season length was consistently longer than in situ data, with a RMSE of 65–102 days and mean bias error of 45 to 96 days¹⁵⁰. For the period 2001–2014, MODIS EVI2-derived SOS advanced by about 2.36 days from middle to high latitudes of Northern Hemisphere (43.5°N – 70.0°N) snow-covered landmass, while it was delayed by about 0.53 days in lower

latitudes (33.0°N – 43.5°N). The differences between MODIS EVI2-derived and in situ SOS at 420 phenology observations from five field datasets, including the Pan European Phenology (PEP) project^{151,152}, are centralized between ± 30 days with a RMSE of 12.13 days and bias of -3.99 days¹⁵³.

Notable limitations of VIs

Although VIs provide valuable insights into vegetation dynamics and changes, there are also limitations in their use, beyond the artefacts described previously. In principle, VIs capture a combination of canopy properties and other external contributing factors, such as atmospheric conditions and sun–target–sensor geometry that can simultaneously and non-uniquely vary throughout the vegetation growing season. Thus, it might not be feasible to relate a VI to a specific plant variable without accounting for changes due to these factors and changing vegetation conditions at the same time. For example, a VI cannot be coupled to leaf biomass without accounting for simultaneous differences in leaf biochemical constituent differences, non-photosynthetic vegetation (NPV), soil background, atmospheric contamination and canopy structural effects, which are also tightly connected to the sun–target–sensor geometry effects. Based on their underlying mathematical basis (TABLE 1), many ratio-based VIs (including NDVI, SR, PRI, CCI and CIred-edge) are sensitive to varying soil brightness owing to larger variation of the denominator than the numerator³, but are insensitive to fractional vegetation cover when the background is dark soil or water¹⁵⁴. For example, a leaf floating in a black waterbody would maintain the same NDVI regardless of how large the leaf became. In other words, the NDVI is the same whether that leaf occupies 1% of the water or 100% of the water (FIG. 4).

The impacts of some inherent properties of vegetation, such as the leaf biochemical constituents and NPV, are usually difficult to separate from green vegetation biophysical properties such as LAI because of limited understanding of their spatio-temporal variations. Leaf biochemical constituents, such as chlorophyll, water and dry matter content, largely determine the leaf reflectance spectrum and, thus, fundamentally shape the vegetation canopy reflectance^{155,156}. However, the strong spatio-temporal variations of leaf biochemical constituents^{57,157} and NPV (including woody stems, branches and standing litter)¹⁵⁸ can mask emerging green vegetation, weakening the correlation between VIs and green vegetation biophysical properties. As a result, phenology could appear delayed owing to the masking by NPV if the standing plant materials from the previous year occlude the initial green-up of vegetation¹⁵⁸. The limitations of VIs can be at least partially addressed when the VI formulae are appropriately designed with the principles of radiative transfer in vegetation canopies (Supplementary information).

Intrinsic similarities between VIs

Although various VIs have been invented, several of the most widely used VIs, particularly those calculated with red and NIR reflectance (NDVI, DVI, EVI, EVI2 and

NIRv), are generally mathematically related. Usually, surface reflectance in the NIR band is larger than that in the red band. In addition, canopy NIR reflectance essentially increases with LAI, while red reflectance shows the opposite trend owing to strong light absorption at this wavelength. Therefore, in the red–NIR VIs, NIR typically dominates the factor $\text{NIR}/(\text{NIR} + \text{Red})$, which equals NIRv/DVI and typically falls in a small range of 0.8–1 for vegetated surfaces ($\text{LAI} > 1$). Therefore, Eq. 2 in BOX 1 suggests that NIRv is well correlated with DVI in most cases, and NIRv has the biophysical meaning of FPAR times photon escape probability (f_{esc}) (FIG. 3).

EVI has been reported to be well approximated by EVI2, a variant of EVI without the blue band²⁷. EVI and EVI2 can be derived as the product of DVI and $2.5/(\text{NIR} + 6\cdot\text{Red} + 7.5\cdot\text{Blue} + 1)$ or $2.5/(\text{NIR} + 2.4\cdot\text{Red} + 1)$ (BOX 1, Eqs 3 and 4), respectively²⁷. The number ‘1’ in the denominator is typically much larger than the variability of the remaining term ($\text{NIR} + 2.4\cdot\text{Red}$) or ($\text{NIR} + 6\cdot\text{Red} + 7.5\cdot\text{Blue}$) in response to the changes of LAI. Thus, the factor $1/(\text{NIR} + 6\cdot\text{Red} + 7.5\cdot\text{Blue} + 1)$ (Eq. 3) is typically between 0.7 and 0.8 in most cases, especially when LAI is greater than 1. Similarly, the factor $1/(\text{NIR} + 2.4\cdot\text{Red} + 1)$ is also almost a constant, with small variation between 0.7 and 0.8 in most cases. This fact suggests that EVI2 and EVI should have a strong linear correlation with DVI, although with different magnitudes because of the constant coefficient (2.5) used in the numerator. The parameters in all of these VIs could be sensor-specific, though.

As DVI is strongly correlated to both EVI and NIRv, NIRv, DVI, EVI and EVI2 intrinsically have strong linear correlations owing to their mathematical definitions and typical range of variation of NIR and VIS reflectance of vegetated surfaces. In contrast, DVI is mathematically the numerator of NDVI, and the denominator ($\text{NIR} + \text{Red}$) can vary significantly with LAI and other vegetation properties. Therefore, a non-linear relationship is often observed between NDVI and DVI, and, thereby, also between NDVI and the other indices similar to DVI, such as EVI, EVI2 and NIRv.

NDVI, EVI and DVI can also be more generally described by another well-known VI, the SAVI, and the ‘L’ in the denominator of SAVI (BOX 1, Eq. 7) is the canopy background adjustment term that addresses the non-linear, differential NIR and red radiative transfer process through a canopy^{4,25}. In case L in SAVI is 0, SAVI is equal to NDVI; if L is 1, SAVI is equal to EVI. Note that factors of 6 and 7.5 in the denominator of EVI (BOX 1, Eq. 3) and 2.4 in the denominator of EVI2 (BOX 1, Eq. 4) are for atmosphere self-correction instead of canopy biophysical properties. When L is infinity, SAVI is equal to DVI. The real canopy has an L value generally greater than 0 but less than 10 (Supplementary information).

Appropriate use of VIs

There is no single best VI; instead, identifying the target application and corresponding sensitive wavelength and VI is the first step towards their optimal use. For example, red–NIR VIs such as NDVI and EVI might be the best choices for studying dynamics of vegetation structure, red-edge VIs are more suitable

Box 1 | Linkages and differences between vegetation indices and solar-induced chlorophyll fluorescence

The difference vegetation index (DVI) is defined as the difference between the near infrared (NIR) and red bands¹⁹:

$$\text{DVI} = \text{NIR} - \text{Red} \quad (1)$$

The linkage between near-infrared reflectance of vegetation (NIRv) and other vegetation indices such as DVI, enhanced vegetation index (EVI) and two-band version of the enhanced vegetation index (EVI2) can be demonstrated by using DVI as the bridge between them. NIRv can be derived as the product of DVI and $\text{NIR}/(\text{NIR} + \text{Red})^5$.

$$\text{NIRv} = \text{NDVI} \cdot \text{NIR} = \frac{\text{NIR} - \text{Red}}{\text{NIR} + \text{Red}} \cdot \text{NIR} = \text{DVI} \cdot \frac{\text{NIR}}{\text{NIR} + \text{Red}} \sim \text{DVI} \quad (2)$$

$$\text{EVI} = 2.5 \cdot \frac{\text{NIR} - \text{Red}}{\text{NIR} + 6 \cdot \text{Red} - 7.5 \cdot \text{Blue} + 1} = \text{DVI} \cdot \frac{2.5}{\text{NIR} + 6 \cdot \text{Red} - 7.5 \cdot \text{Blue} + 1} \sim \text{DVI} \quad (3)$$

$$\text{EVI2} = 2.5 \cdot \frac{\text{NIR} - \text{Red}}{\text{NIR} + 2.4 \cdot \text{Red} + 1} = \text{DVI} \cdot \frac{2.5}{\text{NIR} + 2.4 \cdot \text{Red} + 1} \sim \text{DVI} \quad (4)$$

Shown below is the linkage and difference between the normalized difference vegetation index (NDVI), simple ratio (SR) and soil-adjusted vegetation index (SAVI). Note that when L in SAVI is 0, SAVI is equal to NDVI.

$$\text{NDVI} = \frac{\text{NIR} - \text{Red}}{\text{NIR} + \text{Red}} = \frac{\text{SR} - 1}{\text{SR} + 1} = 1 - \frac{2}{\text{SR} + 1} \quad (5)$$

$$\text{SR} = \text{NIR}/\text{Red} \quad (6)$$

$$\text{SAVI} = (1 + L) \cdot \frac{\text{NIR} - \text{Red}}{\text{NIR} + \text{Red} + L} \quad (7)$$

Based on spectral invariants theory, NIRv and photosynthetically active radiation (PAR)-normalized solar-induced chlorophyll fluorescence (SIF/PAR) can be modelled with similar formulae⁹⁰:

$$\text{NIRv} = \text{FPAR} \cdot \omega \cdot fesc \quad (8)$$

$$\text{SIF/PAR} = \text{FPAR} \cdot \Phi_F \cdot fesc \quad (9)$$

where $fesc$ is the photon escape probability from the canopy, ω is the leaf single scattering albedo in the NIR band, which is close to 1 in the NIR band, Φ_F is the fluorescence yield and FPAR is the fraction of absorbed photosynthetically active radiation. Rearranging Eqs 8 and 9 gives

$$\text{NIRv} : (\text{SIF/PAR}) = \omega : \Phi_F \quad (10)$$

for pigment retrievals and VIS-based PRI and CCI are more appropriate for monitoring physiological changes. Understanding the intrinsic differences, strengths and, particularly, the limitations of VIs will help to further identify the suitable VI or VIs for the application. For example, NDVI could better estimate fractional vegetation cover, as it is less impacted by sun-target-sensor geometry than EVI and NIRv. However, if the sun-target-sensor geometry effect is properly addressed, NDVI could be less robust in estimating fractional vegetation cover owing to its stronger sensitivity to soil brightness changes from rainfall or snowfall³⁴. In addition, VIs are typically saturated in dense vegetated areas; the saturation point of NDVI is usually lower than that of EVI^{25,27}, suggesting that NDVI could be a less appropriate choice for analysing vegetation variations in dense vegetation canopies, whereas NDVI is still useful for onset and offset phenology detection. Even though EVI, EVI2, DVI and NIRv show high correlations, the

mechanistic link that was established between NIRv and the product of FPAR times $fesc$ (FIG. 3) makes NIRv an attractive choice for studies related to GPP estimation and SIF^{90,92,159,160}.

Potential artefacts must be carefully addressed to avoid biased interpretations of the underlying ecological processes resulting from the use of incorrect data. For example, owing to sensor degradation, analysing interannual variations and long-term trends in VIs remained challenging until the inter-calibration of AVHRR with MODIS became feasible in 2000 (REF¹¹²). The newer versions of VI products should theoretically be more accurate than the older ones¹¹⁹. Spectral response function normalizations are recommended for multisensor VI harmonizations¹⁰⁸. The BRDF correction by the kernel-driven model is recommended, especially if the BRDF varies seasonally and latitudinally in the analysis¹²⁸. If uncertainties from sensor calibration¹¹⁸, atmospheric, BRDF and topographic effects¹⁴¹ are a serious issue, ratio-based VIs are recommended over difference-based VIs. Conversely, ratio-based VIs could be sensitive to snow and soil background¹³⁸ and scale effects⁶⁵, which should be considered if the area of interest has substantial background. For spatial aggregation, it is highly recommended to first aggregate the single-band reflectance to coarse resolution and then calculate VIs such as NDVI and EVI, instead of aggregating the high-resolution VIs directly. This practice will avoid the scale effect over heterogeneous surfaces due to possible non-linear formulae of VIs⁶⁵. Fortunately, many well calibrated, processed and harmonized VI products have become available, although users should still carefully understand what artefacts are addressed in these products and what are not¹⁶¹.

Identifying dominant variables and potential signal contamination sources in specific ecosystems is also crucial for the correct use of VIs. For example, for temperate evergreen forests, the structure and chlorophyll in winter might not be very variable, so physiologically associated VIs such as PRI and CCI (which are more sensitive to LUE) should be more suitable^{50,51}. Observations of tropical rainforests could be more vulnerable to atmosphere and optical signal saturation impacts¹²², so EVI is recommended instead of NDVI. Savannah and shrublands with sparse vegetation observations are more sensitive to soil backgrounds²⁵, so EVI and NIRv are recommended. PPI, EVI2 and NIRv with BRDF correction are recommended for high-latitude studies, where observations are vulnerable to large solar zenith angle and ice and snow backgrounds¹³⁸. In mountainous regions with rugged terrain, such as the Tibetan Plateau, ice and snow, topographic and shadowing effects¹⁴⁹ can all be important, so topographic normalizations such as the empirical, semi-empirical and physically based methods¹⁶² are recommended.

Summary and future perspectives

VIs are classic remote-sensing products with a rich research history. Because of their simplicity and robustness, we envision that they will continue to be heavily used in the foreseeable future. However, factors such as the formulation of VIs, sensor characteristics, product

version, compositing algorithms, QA/QC, atmospheric and topographic conditions, and sun-target-sensor geometries all impact VIs and their appropriate use. We strongly recommend that future studies using VIs should be conducted with careful attention to VI interpretation and use more than one in situ dataset for verification when possible to render greater confidence in their findings and conclusions. Looking forward, we identify research opportunities and challenges that could advance the use of VIs in monitoring terrestrial ecosystems from space.

Multisensor fusion of observations can improve the time span and spatio-temporal resolution and continuity of VIs, such as Sentinel-2 and Landsat-8 (REF.¹⁶³), greatly enhancing their applicability. Ongoing efforts are devoted to developing fusion algorithms^{164–167} and datasets^{126,161,168} for producing long-term, gap-free VIs at relatively high resolutions. However, land surface heterogeneity¹⁶⁹ and BRDF effects¹²⁵ remain major challenges that must be resolved, possibly with higher-spatial-resolution and multi-angular observations. Similarly, atmospheric correction deserves greater attention, because even under the same solar angle, VIs vary depending on the fraction of diffuse radiation, which differs at the overpass times of different sensors. Sensor calibration drift and degradation are also critical challenges for the fusion of VI data from similar sensors on multiple satellites or multiple sensors on different satellites, such as AVHRR and MODIS, in producing decadal datasets and analyses^{112,113}.

Most VIs are good proxies of vegetation biophysical properties and, to a limited extent, represent vegetation functioning. Some novel remote-sensing indicators, such as solar-induced chlorophyll fluorescence (SIF)^{170–173}, could provide valuable complementary information. SIF captures some of the vegetation physiological information, and, thus, responds to the onset of environmental conditions and stresses earlier than VIs¹⁷⁴. For example, SIF can track the photosynthetic seasonality in evergreen species in cold environments where red-NIR VIs showed no changes¹⁷⁵. In addition, SIF is rarely impacted by soil because green vegetation is the only source of SIF.

However, the existing SIF retrievals have poor spatial resolution, infrequent revisiting time, low signal-to-noise ratio and a relatively short history of measurements¹⁷⁶. New sensors will continue to enhance the capability for SIF measurements, but complementary VIs such as NIRv provide far better spatial and temporal resolutions. Therefore, understanding the intrinsic linkage between SIF and VIs is key in their synergistic use. Far-red SIF normalized by photosynthetically active radiation (SIF/PAR) and NIRv share the same *fesc* in the radiative transfer process^{90,177} (BOX 1). So, under low-stress conditions with stable fluorescence yield (Φ_F), NIRv and SIF/PAR are expected to be strongly correlated under the same sun-target-sensor geometry (Supplementary Fig. 1). NIRv radiance ($NDVI \times$ NIR radiance) or $NIRvP$ ($NIRv \times$ PAR) and SIF should be even more strongly related than $NIRv$ and SIF/PAR, as the common radiation factor further enhances the underlying relationship^{5,91,159}. The similarity between NIRv and SIF implies that VIs could be used as structural proxies for

SIF because they have a longer data record. For example, MODIS EVI has been used to generate a global SIF product (GOSIF; 2000–2020) from OCO-2 SIF soundings¹⁷⁸. Combining NIRv with SIF during times of the overlapping data has great potential to isolate the unique physiological responses of SIF, as NIRv can be used to normalize the dominant canopy structure effects^{159,179}.

Besides optical data, VIs can also be derived from microwave remote-sensing data. Microwave VIs derived from different frequency and polarization combinations are more sensitive to the woody part of the vegetation than optical VIs such as NDVI¹⁸⁰, and are potential ways to derive vegetation optical depth (VOD)¹⁸¹. VOD describes vegetation extinction effects in the microwave spectrum and is increasingly used for estimating parameters of vegetation water content and the above-ground biomass^{182,183}. It has the advantage of being unaffected by the clouds and is less sensitive to the water in the atmosphere, which is important especially for cloudy and humid tropical regions such as the Amazon and Congo rainforests^{182,184}. VOD has been reported to have a saturation point with higher biomass values than NDVI¹⁸⁴. Therefore, optical VIs with a higher spatial resolution can contribute to the downscaling of VOD, and VOD can help to improve the temporal observing frequency over cloudy and humid regions and seasons.

In addition, hyperspectral data with more spectral details can provide more useful information that is not possible with multispectral data. For example, the widely used red-NIR VIs do not directly contain the LUE information, which can be captured to some degree by PRI⁴⁹ from emerging hyperspectral remote-sensing capabilities. Hyperspectral data can be beneficial for the disentangling of the pure vegetation and soil reflectance contributions in the mixed pixel spectrum, by the newly proposed hyperspectral NIR reflectance of vegetation (NIRvH)¹⁶⁰. The next generation of VIs aim to reduce soil, snow and ice background effects, BRDF impact and signal saturation. Such hyperspectral remote-sensing capability has been limited at the global scale and relatively fine spatial resolution. However, these limitations will be addressed with the emerging and forthcoming space-borne hyperspectral satellite missions such as the HISUI, PRISMA, EnMap, CHIME, DESIS, GeoCarb and SBG. New opportunities to further improve temporal characteristics of traditional VIs will also be provided by the new-generation geostationary satellites, such as GOES, Himawari and GEO-KOMPSAT, as well as the unique DSCOVR mission at the Sun–Earth L1 Lagrange Point, one of the gravitational and orbital equilibrium points between the Earth and the Sun. They provide higher observing frequencies that support not only the diurnal variations of ecosystem processes¹⁸⁵ but also the seasonality of greenness in cloudy and humid regions, such as the Amazon, compared with polar-orbiting satellites^{186,187}.

Finally, it is key to provide detailed documentation of the important processing steps in studies that include VIs, which will facilitate the interpretation and reproducibility of VI-based results. Ideally, the programming code should also be provided as supplemental material or archived in a repository, and, where feasible,

the final VI dataset should be stored in a publicly accessible repository or cloud storage such as Google Earth Engine for ease of access¹⁸⁸. In particular, the documentation should include relevant information on the application of QA/QC levels as well as any other processing steps such as spatio-temporal aggregation, additional quality and outlier filtering or other corrections applied

to the original data. Providing such detailed technical information on VI products might be a promising strategy to further boost confidence, use and reproducibility of remotely sensed vegetation information and broad downstream applications.

Published online: 31 May 2022

1. Houborg, R., Fisher, J. B. & Skidmore, A. K. Advances in remote sensing of vegetation function and traits. *Int. J. Appl. Earth Obs. Geoinf.* **43**, 1–6 (2015).
2. Bannari, A., Morin, D., Bonn, F. & Huete, A. A review of vegetation indices. *Remote Sens. Rev.* **13**, 95–120 (1995).
3. Gao, X., Huete, A. R., Ni, W. & Miura, T. Optical–biophysical relationships of vegetation spectra without background contamination. *Remote Sens. Environ.* **74**, 609–620 (2000).
4. Huete, A. R. A soil-adjusted vegetation index (SAVI). *Remote Sens. Environ.* **25**, 295–309 (1988).
5. Badgley, G., Field, C. B. & Berry, J. A. Canopy near-infrared reflectance and terrestrial photosynthesis. *Sci. Adv.* **3**, e1602244 (2017).
6. Gamon, J. A. et al. A remotely sensed pigment index reveals photosynthetic phenology in evergreen conifers. *Proc. Natl. Acad. Sci. USA* **113**, 13087–13092 (2016).
7. Joiner, J. et al. Estimation of terrestrial global gross primary production (GPP) with satellite data-driven models and eddy covariance flux data. *Remote Sens.* **10**, 1346 (2018).
8. Piao, S. et al. Characteristics, drivers and feedbacks of global greening. *Nat. Rev. Earth Environ.* **1**, 14–27 (2020).
9. Tian, F. et al. Evaluating temporal consistency of long-term global NDVI datasets for trend analysis. *Remote Sens. Environ.* **163**, 326–340 (2015).
10. Fan, X. & Liu, Y. A global study of NDVI difference among moderate-resolution satellite sensors. *ISPRS J. Photogramm. Remote Sens.* **121**, 177–191 (2016).
11. Aghakouchak, A. et al. Remote sensing of drought: progress, challenges and opportunities. *Rev. Geophys.* **53**, 452–480 (2015).
12. Anyamba, A. & Tucker, in *Remote Sensing of Drought: Innovative Monitoring Approaches* Ch. 2 (eds Wardlow, B. D., Anderson, M. C. & Verdin, J. P.) (Taylor & Francis, 2012).
13. Veraverbeke, S. et al. Hyperspectral remote sensing of fire: state-of-the-art and future perspectives. *Remote Sens. Environ.* **216**, 105–121 (2018).
14. Tucker, C. J. Red and photographic infrared linear combinations for monitoring vegetation. *Remote Sens. Environ.* **8**, 127–150 (1979).
15. Rouse, J. W., Haas, R. H., Schell, J. A. & Deering, D. W. Monitoring vegetation systems in the Great Plains with ERTS. *NASA Spec. Publ.* **351**, 309 (1974).
16. Rouse, J. W., Haas, R. H., Schell, J. A., Deering, D. W. & Harlan, J. C. Monitoring the vernal advancement and retrogradation (green wave effect) of natural vegetation. *NASA/GSFC Type III Final Report*, 371 (NASA, 1974).
17. Gutman, G., Skakun, S. & Gitelson, A. Revisiting the use of red and near-infrared reflectances in vegetation studies and numerical climate models. *Sci. Remote Sens.* **4**, 100025 (2021).
18. Jackson, R. D. & Huete, A. R. Interpreting vegetation indices. *Prev. Vet. Med.* **11**, 185–200 (1991).
19. Richardson, A. J. & Wiegand, C. Distinguishing vegetation from soil background information. *Photogramm. Eng. Remote Sens.* **43**, 1541–1552 (1977).
20. Baret, F., Guyot, G. & Major, D. in *12th Canadian Symposium on Remote Sensing Geoscience and Remote Sensing Symposium* 1355–1358 (IEEE, 1989).
21. Qi, J., Chehbouni, A., Huete, A. R., Kerr, Y. H. & Sorooshian, S. A modified soil adjusted vegetation index. *Remote Sens. Environ.* **48**, 119–126 (1994).
22. Chen, J. M. Evaluation of vegetation indices and a modified simple ratio for boreal applications. *Can. J. Remote Sens.* **22**, 229–242 (1996).
23. Brown, L., Chen, J. M., Leblanc, S. G. & Cihlar, J. A shortwave infrared modification to the simple ratio for LAI retrieval in boreal forests: an image and model analysis. *Remote Sens. Environ.* **71**, 16–25 (2000).
24. Pinty, B. & Verstraete, M. GEMI: a non-linear index to monitor global vegetation from satellites. *Vegetatio* **101**, 15–20 (1992).
25. Huete, A. et al. Overview of the radiometric and biophysical performance of the MODIS vegetation indices. *Remote Sens. Environ.* **83**, 195–213 (2002).
26. Kaufman, Y. J. & Tanre, D. Atmospherically resistant vegetation index (ARVI) for EOS-MODIS. *IEEE Trans. Geosci. Remote Sens.* **30**, 261–270 (1992).
27. Jiang, Z., Huete, A. R., Didan, K. & Miura, T. Development of a two-band enhanced vegetation index without a blue band. *Remote Sens. Environ.* **112**, 3833–3845 (2008).
28. Jin, H. & Eklundh, L. A physically based vegetation index for improved monitoring of plant phenology. *Remote Sens. Environ.* **152**, 512–525 (2014).
29. Yang, P., van der Tol, C., Campbell, P. K. & Middleton, E. M. Fluorescence Correction Vegetation Index (FCVI): A physically based reflectance index to separate physiological and non-physiological information in far-red sun-induced chlorophyll fluorescence. *Remote Sens. Environ.* **240**, 111676 (2020).
30. Badgley, G., Anderegg, L. D., Berry, J. A. & Field, C. B. Terrestrial gross primary production: Using NIR_v to scale from site to globe. *Glob. Change Biol.* **25**, 3731–3740 (2019).
31. Camps-Valls, G. et al. A unified vegetation index for quantifying the terrestrial biosphere. *Sci. Adv.* **7**, eabc7447 (2021).
32. Roberts, D. A., Roth, K. L. & Perroy, R. L. in *Hyperspectral Remote Sensing of Vegetation* Ch. 14 (eds Thenkabail, P. S., Lyon, J. G. & Huete, A.) (CRC, 2016).
33. Gitelson, A. A., Vina, A., Ciganda, V., Rundquist, D. C. & Arkebauer, T. J. Remote estimation of canopy chlorophyll content in crops. *Geophys. Res. Lett.* **32**, L08403 (2005).
34. Gitelson, A. & Merzlyak, M. N. Spectral reflectance changes associated with autumn senescence of *Aesculus hippocastanum* L. and *Acer platanoides* L. leaves. Spectral features and relation to chlorophyll estimation. *J. Plant Physiol.* **143**, 286–292 (1994).
35. Dash, J. & Curran, P. The MERIS terrestrial chlorophyll index. *Int. J. Remote Sens.* **25**, 5403–5413 (2004).
36. Penuelas, J., Baret, F. & Filella, I. Semi-empirical indices to assess carotenoids/chlorophyll a ratio from leaf spectral reflectance. *Photosynthetica* **31**, 221–230 (1995).
37. Penuelas, J., Gamon, J., Fredeen, A., Merino, J. & Field, C. Reflectance indices associated with physiological changes in nitrogen- and water-limited sunflower leaves. *Remote Sens. Environ.* **48**, 135–146 (1994).
38. Merzlyak, M. N., Gitelson, A. A., Chivkunova, O. B. & Rakitin, V. Y. Non-destructive optical detection of pigment changes during leaf senescence and fruit ripening. *Physiol. Plant.* **106**, 135–141 (1999).
39. Gitelson, A. A., Merzlyak, M. N. & Chivkunova, O. B. Optical properties and nondestructive estimation of anthocyanin content in plant leaves. *Photochem. Photobiol.* **74**, 38–45 (2001).
40. van den Berg, A. K. & Perkins, T. D. Nondestructive estimation of anthocyanin content in autumn sugar maple leaves. *HortScience* **40**, 685–686 (2005).
41. Gamon, J. & Surfus, J. Assessing leaf pigment content and activity with a reflectometer. *New Phytol.* **143**, 105–117 (1999).
42. Gao, B.-C. NDWI — a normalized difference water index for remote sensing of vegetation liquid water from space. *Remote Sens. Environ.* **58**, 257–266 (1996).
43. Xiao, X., Boles, S., Liu, J., Zhuang, D. & Liu, M. Characterization of forest types in Northeastern China, using multi-temporal SPOT-4 VEGETATION sensor data. *Remote Sens. Environ.* **82**, 335–348 (2002).
44. Xiao, X. et al. Satellite-based modeling of gross primary production in an evergreen needleleaf forest. *Remote Sens. Environ.* **89**, 519–534 (2004).
45. Yilmaz, M. T., Hunt, E. R. Jr & Jackson, T. J. Remote sensing of vegetation water content from equivalent water thickness using satellite imagery. *Remote Sens. Environ.* **112**, 2514–2522 (2008).
46. Cheng, Y.-B., Ustin, S. L., Riaño, D. & Vanderbilt, V. C. Water content estimation from hyperspectral images and MODIS indexes in Southeastern Arizona. *Remote Sens. Environ.* **112**, 363–374 (2008).
47. Serrano, L., Penuelas, J. & Ustin, S. L. Remote sensing of nitrogen and lignin in Mediterranean vegetation from AVIRIS data: decomposing biochemical from structural signals. *Remote Sens. Environ.* **81**, 355–364 (2002).
48. Filella, I. et al. PRI assessment of long-term changes in carotenoids/chlorophyll ratio and short-term changes in de-epoxidation state of the xanthophyll cycle. *Int. J. Remote Sens.* **30**, 4443–4455 (2009).
49. Gamon, J., Penuelas, J. & Field, C. A narrow-waveband spectral index that tracks diurnal changes in photosynthetic efficiency. *Remote Sens. Environ.* **41**, 35–44 (1992).
50. Cheng, R. et al. Decomposing reflectance spectra to track gross primary production in a subalpine evergreen forest. *Biogeosciences* **17**, 4523–4544 (2020).
51. Seyednasrollah, B. et al. Seasonal variation in the canopy color of temperate evergreen conifer forests. *New Phytol.* **229**, 2586–2600 (2021).
52. Merton, R. in *Proceedings of the Seventh Annual JPL Airborne Earth Science Workshop* 12–16 (NASA, 2004).
53. Naidu, R. A., Perry, E. M., Pierce, F. J. & Mekuria, T. The potential of spectral reflectance technique for the detection of *Grapevine leafroll-associated virus-3* in two red-berried wine grape cultivars. *Comput. Electron. Agric.* **66**, 38–45 (2009).
54. Chen, Y. et al. Generation and evaluation of LAI and FPAR products from Himawari-8 Advanced Himawari imager (AHI) data. *Remote Sens.* **11**, 1517 (2019).
55. Zhu, Z. et al. Global data sets of vegetation leaf area index (LAI)3g and fraction of photosynthetically active radiation (FPAR)3g derived from global inventory modeling and mapping studies (GIMMS) normalized difference vegetation index (NDVI3g) for the period 1981 to 2011. *Remote Sens.* **5**, 927–948 (2013).
56. Liu, Y., Liu, R. & Chen, J. M. Retrospective retrieval of long-term consistent global leaf area index (1981–2011) from combined AVHRR and MODIS data. *J. Geophys. Res.* **117**, G04003 (2012).
57. Croft, H. et al. The global distribution of leaf chlorophyll content. *Remote Sens. Environ.* **236**, 111479 (2020).
58. Bayat, B. et al. Toward operational validation systems for global satellite-based terrestrial essential climate variables. *Int. J. Appl. Earth Obs. Geoinf.* **95**, 102240 (2021).
59. Cui, Y., Song, L. & Fan, W. Generation of spatio-temporally continuous evapotranspiration and its components by coupling a two-source energy balance model and a deep neural network over the Heihe River Basin. *J. Hydrol.* **597**, 126176 (2021).
60. Ali, I., Greifeneder, F., Stamenovic, J., Neumann, M. & Notarnicola, C. Review of machine learning approaches for biomass and soil moisture retrievals from remote sensing data. *Remote Sens.* **7**, 16398–16421 (2015).
61. Gitelson, A. A. et al. Remote estimation of leaf area index and green leaf biomass in maize canopies. *Geophys. Res. Lett.* **30**, 1248 (2003).
62. Huang, M. et al. Air temperature optima of vegetation productivity across global biomes. *Nat. Ecol. Evol.* **3**, 772–779 (2019).
63. Wang, S. et al. Recent global decline of CO₂ fertilization effects on vegetation photosynthesis. *Science* **370**, 1295–1300 (2020).
64. Morton, D. C. et al. Amazon forests maintain consistent canopy structure and greenness during the dry season. *Nature* **506**, 221–224 (2014).
65. Jiang, Z. et al. Analysis of NDVI and scaled difference vegetation index retrievals of vegetation fraction. *Remote Sens. Environ.* **101**, 366–378 (2006).
66. Haboudane, D., Miller, J. R., Pattee, E., Zarco-Tejada, P. J. & Strachan, I. B. Hyperspectral vegetation indices and novel algorithms for predicting green LAI of crop

TECHNICAL REVIEWS

- canopies: modeling and validation in the context of precision agriculture. *Remote Sens. Environ.* **90**, 337–352 (2004).
67. Wu, C., Wang, L., Niu, Z., Gao, S. & Wu, M. Nondestructive estimation of canopy chlorophyll content using Hyperion and Landsat/TM images. *Int. J. Remote Sens.* **31**, 2159–2167 (2010).
 68. Wang, R. & Gamon, J. A. Remote sensing of terrestrial plant biodiversity. *Remote Sens. Environ.* **231**, 111218 (2019).
 69. Ustin, S. L. & Gamon, J. A. Remote sensing of plant functional types. *New Phytol.* **186**, 795–816 (2010).
 70. Hilker, T. et al. Vegetation dynamics and rainfall sensitivity of the Amazon. *Proc. Natl Acad. Sci. USA* **111**, 16041–16046 (2014).
 71. Zhang, Y., Commane, R., Zhou, S., Williams, A. P. & Gentile, P. Light limitation regulates the response of autumn terrestrial carbon uptake to warming. *Nat. Clim. Change* **10**, 739–743 (2020).
 72. Weber, M. et al. Exploring the use of DSCOVR/EPIC satellite observations to monitor vegetation phenology. *Remote Sens.* **12**, 2384 (2020).
 73. Ganguly, S., Friedl, M. A., Tan, B., Zhang, X. & Verma, M. Land surface phenology from MODIS: characterization of the Collection 5 global land cover dynamics product. *Remote Sens. Environ.* **114**, 1805–1816 (2010).
 74. Gray, J., Sulla-Menashe, D. & Friedl, M. A. *User Guide to Collection 6 MODIS Land Cover Dynamics Product (MCD12Q2)* (NASA, 2019).
 75. Wang, S., Zhang, Y., Ju, W., Qiu, B. & Zhang, Z. Tracking the seasonal and inter-annual variations of global gross primary production during last four decades using satellite near-infrared reflectance data. *Sci. Total Environ.* **755**, 142569 (2021).
 76. Tian, F. et al. Calibrating vegetation phenology from Sentinel-2 using eddy covariance, PhenoCam, and PEP725 networks across Europe. *Remote Sens. Environ.* **260**, 112456 (2021).
 77. Yin, G., Verger, A., Filella, I., Descals, A. & Peñuelas, J. Divergent estimates of forest photosynthetic phenology using structural and physiological vegetation indices. *Geophys. Res. Lett.* **47**, e2020GL089167 (2020).
 78. Qin, Y. et al. Carbon loss from forest degradation exceeds that from deforestation in the Brazilian Amazon. *Nat. Clim. Change* **11**, 442–448 (2021).
 79. Samanta, A. et al. Amazon forests did not green-up during the 2005 drought. *Geophys. Res. Lett.* **37**, L05401 (2010).
 80. Shi, Y., Huang, W., Luo, J., Huang, L. & Zhou, X. Detection and discrimination of pests and diseases in winter wheat based on spectral indices and kernel discriminant analysis. *Comput. Electron. Agric.* **141**, 171–180 (2017).
 81. Zhang, Z., Liu, M., Liu, X. & Zhou, G. A new vegetation index based on multitemporal Sentinel-2 images for discriminating heavy metal stress levels in rice. *Sensors* **18**, 2172 (2018).
 82. Yengoh, G. T., Dent, D., Olsson, L., Tengberg, A. E. & Tucker III, C. J. *Use of the Normalized Difference Vegetation Index (NDVI) to Assess Land Degradation at Multiple Scales: Current Status, Future Trends, and Practical Considerations* (Springer, 2015).
 83. Potter, C. S. et al. Terrestrial ecosystem production: a process model based on global satellite and surface data. *Glob. Biogeochem. Cycles* **7**, 811–841 (1993).
 84. Running, S. W. et al. A continuous satellite-derived measure of global terrestrial primary production. *Bioscience* **54**, 547–560 (2004).
 85. Yuan, R. et al. Deriving a light use efficiency model from eddy covariance flux data for predicting daily gross primary production across biomes. *Agric. For. Meteorol.* **143**, 189–207 (2007).
 86. Chen, M. et al. Quantification of terrestrial ecosystem carbon dynamics in the conterminous United States combining a process-based biogeochemical model and MODIS and AmeriFlux data. *Biogeosciences* **8**, 2665–2688 (2011).
 87. Xiao, J. et al. A continuous measure of gross primary production for the conterminous United States derived from MODIS and AmeriFlux data. *Remote Sens. Environ.* **114**, 576–591 (2010).
 88. Jiang, C., Guan, K., Wu, G., Peng, B. & Wang, S. A daily, 250 m, and real-time gross primary productivity product (2000–present) covering the contiguous United States. *Earth Syst. Sci. Data Discuss.* **2020**, 1–28 (2020).
 89. Schubert, P. et al. Modeling GPP in the Nordic forest landscape with MODIS time series data — comparison with the MODIS GPP product. *Remote Sens. Environ.* **126**, 136–147 (2012).
 90. Zeng, Y. et al. A practical approach for estimating the escape ratio of near-infrared solar-induced chlorophyll fluorescence. *Remote Sens. Environ.* **232**, 111209 (2019).
 91. Baldocchi, D. D. et al. Outgoing near infrared radiation from vegetation scales with canopy photosynthesis across a spectrum of function, structure, physiological capacity and weather. *J. Geophys. Res.* **125**, e2019JG005534 (2020).
 92. Dechant, B. et al. Canopy structure explains the relationship between photosynthesis and sun-induced chlorophyll fluorescence in crops. *Remote Sens. Environ.* **241**, 111733 (2020).
 93. Rahman, A. F., Gamon, J. A., Fuentes, D. A., Roberts, D. A. & Prentiss, D. Modeling spatially distributed ecosystem flux of boreal forest using hyperspectral indices from AVIRIS imagery. *J. Geophys. Res. Atmos.* **106**, 33579–33591 (2001).
 94. Zhu, Z. et al. Comment on “Recent global decline of CO₂ fertilization effects on vegetation photosynthesis”. *Science* **373**, eabg2947 (2021).
 95. Doughty, R. et al. Small anomalies in dry-season greenness and chlorophyll fluorescence for Amazon moist tropical forests during El Niño and La Niña. *Remote Sens. Environ.* **253**, 112196 (2021).
 96. Huang, N. et al. Spatial and temporal variations in global soil respiration and their relationships with climate and land cover. *Sci. Adv.* **6**, eabb8508 (2020).
 97. Huang, N., He, J.-S. & Niu, Z. Estimating the spatial pattern of soil respiration in Tibetan alpine grasslands using Landsat TM images and MODIS data. *Ecol. Indic.* **26**, 117–125 (2013).
 98. Neale, C. M., Gonzalez-Dugo, M. P., Serrano-Perez, A., Campos, I. & Mateos, L. Cotton canopy reflectance under variable solar zenith angles: implications of use in evapotranspiration models. *Hydrolog. Process.* **35**, e14162 (2021).
 99. Chen, J. M. & Liu, J. Evolution of evapotranspiration models using thermal and shortwave remote sensing data. *Remote Sens. Environ.* **237**, 111594 (2020).
 100. Glenn, E. P., Huete, A. R., Nagler, P. L. & Nelson, S. G. Relationship between remotely-sensed vegetation indices, canopy attributes and plant physiological processes: what vegetation indices can and cannot tell us about the landscape. *Sensors* **8**, 2136–2160 (2008).
 101. Cui, Y., Jia, L. & Fan, W. Estimation of actual evapotranspiration and its components in an irrigated area by integrating the Shuttleworth-Wallace and surface temperature-vegetation index schemes using the particle swarm optimization algorithm. *Agric. For. Meteorol.* **307**, 108488 (2021).
 102. Glenn, E. P., Neale, C. M., Hunsaker, D. J. & Nagler, P. L. Vegetation index-based crop coefficients to estimate evapotranspiration by remote sensing in agricultural and natural ecosystems. *Hydrolog. Process.* **25**, 4050–4062 (2011).
 103. French, A. N. et al. Satellite-based NDVI crop coefficients and evapotranspiration with eddy covariance validation for multiple durum wheat fields in the US Southwest. *Agric. Water Manag.* **239**, 106266 (2020).
 104. Lotsch, A., Friedl, M. A., Anderson, B. T. & Tucker, C. J. Coupled vegetation-precipitation variability observed from satellite and climate records. *Geophys. Res. Lett.* **30**, 1774 (2003).
 105. Nezlin, N. P., Kostianoy, A. G. & Li, B.-L. Inter-annual variability and interaction of remote-sensed vegetation index and atmospheric precipitation in the Aral Sea region. *J. Arid Environ.* **62**, 677–700 (2005).
 106. Notaro, M., Liu, Z. & Williams, J. W. Observed vegetation-climate feedbacks in the United States. *J. Clim.* **19**, 763–786 (2006).
 107. Fensholt, R. & Proud, S. R. Evaluation of earth observation based global long term vegetation trends — Comparing GIMMS and MODIS global NDVI time series. *Remote Sens. Environ.* **119**, 131–147 (2012).
 108. Trishchenko, A. P., Cihlar, J. & Li, Z. Effects of spectral response function on surface reflectance and NDVI measured with moderate resolution satellite sensors. *Remote Sens. Environ.* **81**, 1–18 (2002).
 109. Ustin, S. L. & Middleton, E. M. Current and near-term advances in Earth observation for ecological applications. *Ecol. Process.* **10**, 1 (2021).
 110. Wang, D. et al. Impact of sensor degradation on the MODIS NDVI time series. *Remote Sens. Environ.* **119**, 55–61 (2012).
 111. Zhang, Y., Song, C., Band, L. E., Sun, G. & Li, J. Reanalysis of global terrestrial vegetation trends from MODIS products: browning or greening? *Remote Sens. Environ.* **191**, 145–155 (2017).
 112. Bhatt, R. et al. A consistent AVHRR visible calibration record based on multiple methods applicable for the NOAA degrading orbits. Part I: Methodology. *J. Atmos. Ocean. Technol.* **33**, 2499–2515 (2016).
 113. Frankenberger, C., Yin, Y., Byrne, B., He, L. & Gentile, P. Comment on “Recent global decline of CO₂ fertilization effects on vegetation photosynthesis”. *Science* **373**, eabg2947 (2021).
 114. Los, S. O. Estimation of the ratio of sensor degradation between NOAA AVHRR channels 1 and 2 from monthly NDVI composites. *IEEE Trans. Geosci. Remote Sens.* **36**, 206–213 (1998).
 115. Jiang, C. et al. Inconsistencies of interannual variability and trends in long-term satellite leaf area index products. *Glob. Change Biol.* **23**, 4133–4146 (2017).
 116. de Beurs, K. M. & Henebry, G. M. Trend analysis of the Pathfinder AVHRR Land (PAL) NDVI data for the deserts of Central Asia. *IEEE Geosci. Remote Sens. Lett.* **1**, 282–286 (2004).
 117. Wang, Z. et al. Large discrepancies of global greening: indication of multi-source remote sensing data. *Global Ecol. Conserv.* **34**, e02016 (2022).
 118. Miura, T., Huete, A. R. & Yoshioka, H. Evaluation of sensor calibration uncertainties on vegetation indices for MODIS. *IEEE Trans. Geosci. Remote Sens.* **38**, 1399–1409 (2000).
 119. Lyapustin, A. et al. Scientific impact of MODIS C5 calibration degradation and C6+ improvements. *Atmos. Meas. Tech.* **7**, 4353–4365 (2014).
 120. Buchhorn, M., Raynolds, M. K. & Walker, D. A. Influence of BRDF on NDVI and biomass estimations of Alaska Arctic tundra. *Environ. Res. Lett.* **11**, 125002 (2016).
 121. Fensholt, R., Sandholt, I., Proud, S. R., Stisen, S. & Rasmussen, M. O. Assessment of MODIS sun-sensor geometry variations effect on observed NDVI using MSG SEVIRI geostationary data. *Int. J. Remote Sens.* **31**, 6163–6187 (2010).
 122. Saleska, S. R. et al. Dry-season greening of Amazon forests. *Nature* **531**, E4–E5 (2016).
 123. Lyapustin, A. I. et al. Multi-angle implementation of atmospheric correction for MODIS (MAIAC): 3. Atmospheric correction. *Remote Sens. Environ.* **127**, 385–393 (2012).
 124. Norris, J. R. & Walker, J. J. Solar and sensor geometry, not vegetation response, drive satellite NDVI phenology in widespread ecosystems of the western United States. *Remote Sens. Environ.* **249**, 112013 (2020).
 125. Roy, D. P. et al. A general method to normalize Landsat reflectance data to nadir BRDF adjusted reflectance. *Remote Sens. Environ.* **176**, 255–271 (2016).
 126. Schaaf, C. B. et al. First operational BRDF, albedo nadir reflectance products from MODIS. *Remote Sens. Environ.* **83**, 135–148 (2002).
 127. Didan, K., Munoz, A. B., Solano, R. & Huete, A. *MODIS Vegetation Index User's Guide (MOD13 Series)* (Univ. Arizona, 2015).
 128. Wang, Z., Schaaf, C. B., Sun, O., Shuai, Y. & Román, M. O. Capturing rapid land surface dynamics with Collection V006 MODIS BRDF/NBAR/Albedo (MCD43) products. *Remote Sens. Environ.* **207**, 50–64 (2018).
 129. Saleska, S. R., Didan, K., Huete, A. R. & Da Rocha, H. R. Amazon forests green-up during 2005 drought. *Science* **318**, 612 (2007).
 130. Vargas, M., Miura, T., Shabanov, N. & Kato, A. An initial assessment of Suomi NPP VIIRS vegetation index EDR. *J. Geophys. Res. Atmos.* **118**, 12,301–12,316 (2013).
 131. Kobayashi, H. & Dye, D. G. Atmospheric conditions for monitoring the long-term vegetation dynamics in the Amazon using normalized difference vegetation index. *Remote Sens. Environ.* **97**, 519–525 (2005).
 132. Jiang, C. & Fang, H. GSV: a general model for hyperspectral soil reflectance simulation. *Int. J. Appl. Earth Obs. Geoinf.* **83**, 101932 (2019).
 133. Verrelst, J., Schaepman, M. E., Malenovský, Z. & Clevers, J. G. Effects of woody elements on simulated canopy reflectance: Implications for forest chlorophyll content retrieval. *Remote Sens. Environ.* **114**, 647–656 (2010).
 134. Huete, A. & Tucker, C. Investigation of soil influences in AVHRR red and near-infrared vegetation index imagery. *Int. J. Remote Sens.* **12**, 1223–1242 (1991).
 135. Farrar, T., Nicholson, S. & Lare, A. The influence of soil type on the relationships between NDVI, rainfall, and soil moisture in semiarid Botswana. II. NDVI response to soil moisture. *Remote Sens. Environ.* **50**, 121–133 (1994).

136. Huete, A. & Warrick, A. Assessment of vegetation and soil water regimes in partial canopies with optical remotely sensed data. *Remote Sens. Environ.* **32**, 155–167 (1990).
137. Wang, C. et al. A snow-free vegetation index for improved monitoring of vegetation spring green-up date in deciduous ecosystems. *Remote Sens. Environ.* **196**, 1–12 (2017).
138. Myers-Smith, I. H. et al. Complexity revealed in the greening of the Arctic. *Nat. Clim. Change* **10**, 106–117 (2020).
139. Shen, M. et al. No evidence of continuously advanced green-up dates in the Tibetan Plateau over the last decade. *Proc. Natl Acad. Sci.* **110**, E2329 (2013).
140. Hao, D. et al. Modeling anisotropic reflectance over composite sloping terrain. *IEEE Trans. Geosci. Remote Sens.* **56**, 3903–3923 (2018).
141. Matsushita, B., Yang, W., Chen, J., Onda, Y. & Qiu, G. Sensitivity of the enhanced vegetation index (EVI) and normalized difference vegetation index (NDVI) to topographic effects: a case study in high-density cypress forest. *Sensors* **7**, 2636–2651 (2007).
142. Wen, J. et al. Characterizing land surface anisotropic reflectance over rugged terrain: a review of concepts and recent developments. *Remote Sens.* **10**, 370 (2018).
143. Friedl, M. A., Davis, F. W., Michaelsen, J. & Moritz, M. Scaling and uncertainty in the relationship between the NDVI and land surface biophysical variables: an analysis using a scene simulation model and data from FIFE. *Remote Sens. Environ.* **54**, 233–246 (1995).
144. Tan, B. et al. The impact of gridding artifacts on the local spatial properties of MODIS data: implications for validation, compositing, and band-to-band registration across resolutions. *Remote Sens. Environ.* **105**, 98–114 (2006).
145. Wolfe, R. E. et al. Achieving sub-pixel geolocation accuracy in support of MODIS land science. *Remote Sens. Environ.* **83**, 31–49 (2002).
146. Ferreira, M. P. et al. Retrieving structural and chemical properties of individual tree crowns in a highly diverse tropical forest with 3D radiative transfer modeling and imaging spectroscopy. *Remote Sens. Environ.* **211**, 276–291 (2018).
147. Huete, A. R. et al. Amazon rainforests green-up with sunlight in dry season. *Geophys. Res. Lett.* **33**, L06405 (2006).
148. Herrmann, S. M. & Tappan, G. G. Vegetation impoverishment despite greening: a case study from central Senegal. *J. Arid Environ.* **90**, 55–66 (2013).
149. Wang, X. et al. No consistent evidence for advancing or delaying trends in spring phenology on the Tibetan Plateau. *J. Geophys. Res. Biogeosci.* **122**, 3288–3305 (2017).
150. Donnelly, A., Yu, R. & Liu, L. Comparing in situ spring phenology and satellite-derived start of season at rural and urban sites in Ireland. *Int. J. Remote Sens.* **42**, 7821–7841 (2021).
151. Tempi, B. et al. Pan European Phenological database (PEP725): a single point of access for European data. *Int. J. Biometeorol.* **62**, 1109–1113 (2018).
152. Fu, Y. H. et al. Declining global warming effects on the phenology of spring leaf unfolding. *Nature* **526**, 104–107 (2015).
153. Chen, X. & Yang, Y. Observed earlier start of the growing season from middle to high latitudes across the Northern Hemisphere snow-covered landmass for the period 2001–2014. *Environ. Res. Lett.* **15**, 034042 (2020).
154. Alatorre, L. C. et al. Temporal changes of NDVI for qualitative environmental assessment of mangroves: shrimp farming impact on the health decline of the arid mangroves in the Gulf of California (1990–2010). *J. Arid Environ.* **125**, 98–109 (2016).
155. Jacquemoud, S. & Baret, F. PROSPECT: a model of leaf optical properties spectra. *Remote Sens. Environ.* **34**, 75–91 (1990).
156. Wu, S. et al. Quantifying leaf optical properties with spectral invariants theory. *Remote Sens. Environ.* **253**, 112131 (2021).
157. Wang, Z. et al. Mapping foliar functional traits and their uncertainties across three years in a grassland experiment. *Remote Sens. Environ.* **221**, 405–416 (2019).
158. Van Leeuwen, W. & Huete, A. Effects of standing litter on the biophysical interpretation of plant canopies with spectral indices. *Remote Sens. Environ.* **55**, 123–138 (1996).
159. Dechant, B. et al. NIRvP: a robust structural proxy for sun-induced chlorophyll fluorescence and photosynthesis across scales. *Remote Sens. Environ.* **268**, 112763 (2022).
160. Zeng, Y. et al. Estimating near-infrared reflectance of vegetation from hyperspectral data. *Remote Sens. Environ.* **267**, 112723 (2021).
161. Claverie, M. et al. The Harmonized Landsat and Sentinel-2 surface reflectance data set. *Remote Sens. Environ.* **219**, 145–161 (2018).
162. Hansot, S. & Chuvieco, E. Evaluation of different topographic correction methods for Landsat imagery. *Int. J. Appl. Earth Obs. Geoinf.* **13**, 691–700 (2011).
163. Zhang, H. K. et al. Characterization of Sentinel-2A and Landsat-8 top of atmosphere, surface, and nadir BRDF adjusted reflectance and NDVI differences. *Remote Sens. Environ.* **215**, 482–494 (2018).
164. Gao, F., Masek, J., Schwaller, M. & Hall, F. On the blending of the Landsat and MODIS surface reflectance: predicting daily Landsat surface reflectance. *IEEE Trans. Geosci. Remote Sens.* **44**, 2207–2218 (2006).
165. Zhu, X. et al. A flexible spatiotemporal method for fusing satellite images with different resolutions. *Remote Sens. Environ.* **172**, 165–177 (2016).
166. Luo, Y., Guan, K. & Peng, J. STAIR: A generic and fully automated method to fuse multiple sources of optical satellite data to generate a high-resolution, daily and cloud-gap-free surface reflectance product. *Remote Sens. Environ.* **214**, 87–99 (2018).
167. Houbrug, R. & McCabe, M. F. Daily retrieval of NDVI and LAI at 3 m resolution via the fusion of CubeSat, Landsat, and MODIS data. *Remote Sens.* **10**, 890 (2018).
168. Kimm, H. et al. Deriving high-spatiotemporal-resolution leaf area index for agroecosystems in the US Corn Belt using Planet Labs CubeSat and STAIR fusion data. *Remote Sens. Environ.* **239**, 111615 (2020).
169. Kong, J. et al. Evaluation of four image fusion NDVI products against in-situ spectral-measurements over a heterogeneous rice paddy landscape. *Agric. For. Meteorol.* **297**, 108255 (2021).
170. Köhler, P. et al. Global retrievals of solar-induced chlorophyll fluorescence with TROPOMI: first results and intersensor comparison to OCO-2. *Geophys. Res. Lett.* **45**, 10,456–10,463 (2018).
171. Sun, Y. et al. OCO-2 advances photosynthesis observation from space via solar-induced chlorophyll fluorescence. *Science* **358**, eaam5747 (2017).
172. Joiner, J., Yoshida, Y., Vasilkov, A. & Middleton, E. First observations of global and seasonal terrestrial chlorophyll fluorescence from space. *Biogeosciences* **8**, 637–651 (2011).
173. Frankenberg, C. et al. New global observations of the terrestrial carbon cycle from GOSAT: patterns of plant fluorescence with gross primary productivity. *Geophys. Res. Lett.* **38**, L17706 (2011).
174. Qiu, B., Ge, J., Guo, W., Pitman, A. J. & Mu, M. Responses of Australian dryland vegetation to the 2019 heat wave at a subdaily scale. *Geophys. Res. Lett.* **47**, e2019GL086569 (2020).
175. Magney, T. S. et al. Mechanistic evidence for tracking the seasonality of photosynthesis with solar-induced fluorescence. *Proc. Natl Acad. Sci. USA* **116**, 11640–11645 (2019).
176. Quanter, L. et al. Potential of the TROPOspheric Monitoring Instrument (TROPOMI) onboard the Sentinel-5 Precursor for the monitoring of terrestrial chlorophyll fluorescence. *Atmos. Meas. Tech.* **8**, 1357–1352 (2015).
177. Knyazikhin, Y. et al. Hyperspectral remote sensing of foliar nitrogen content. *Proc. Natl Acad. Sci. USA* **110**, E185–E192 (2013).
178. Li, X. & Xiao, J. A global, 0.05-degree product of solar-induced chlorophyll fluorescence derived from OCO-2, MODIS, and reanalysis data. *Remote Sens.* **11**, 517 (2019).
179. Zeng, Y. et al. Combining near-infrared radiance of vegetation and fluorescence spectroscopy to detect effects of abiotic changes and stresses. *Remote Sens. Environ.* **270**, 112856 (2022).
180. Shi, J. et al. Microwave vegetation indices for short vegetation covers from satellite passive microwave sensor AMSR-E. *Remote Sens. Environ.* **112**, 4285–4300 (2008).
181. Talebianfandarani, S. et al. Microwave vegetation index from multi-angular observations and its application in vegetation properties retrieval: theoretical modelling. *Remote Sens.* **11**, 730 (2019).
182. Wigneron, J.-P. et al. SMOS-IC data record of soil moisture and L-VOD: historical development, applications and perspectives. *Remote Sens. Environ.* **254**, 112238 (2021).
183. Zhang, Y., Zhou, S., Gentile, P. & Xiao, X. Can vegetation optical depth reflect changes in leaf water potential during soil moisture dry-down events? *Remote Sens. Environ.* **234**, 111451 (2019).
184. Frappart, F. et al. Global monitoring of the vegetation dynamics from the vegetation optical depth (VOD): a review. *Remote Sens.* **12**, 2915 (2020).
185. Xiao, J., Fisher, J. B., Hashimoto, H., Ichii, K. & Parazoo, N. C. Emerging satellite observations for diurnal cycling of ecosystem processes. *Nat. Plants* **7**, 877–887 (2021).
186. Hashimoto, H. et al. New generation geostationary satellite observations support seasonality in greenness of the Amazon evergreen forests. *Nat. Commun.* **12**, 684 (2021).
187. Somkuti, P. et al. Solar-induced chlorophyll fluorescence from the Geostationary Carbon Cycle Observatory (GeoCarb): An extensive simulation study. *Remote Sens. Environ.* **263**, 112565 (2021).
188. Gorelick, N. et al. Google Earth Engine: planetary-scale geospatial analysis for everyone. *Remote Sens. Environ.* **202**, 18–27 (2017).
189. Richardson, A. D., Braswell, B. H., Hollinger, D. Y., Jenkins, J. P. & Ollinger, S. V. Near-surface remote sensing of spatial and temporal variation in canopy phenology. *Ecol. Appl.* **19**, 1417–1428 (2009).
190. Daughtry, C. S. Discriminating crop residues from soil by shortwave infrared reflectance. *Agron. J.* **93**, 125–131 (2001).

Acknowledgements

Y.Z. and M.C. acknowledges support from the National Aeronautics and Space Administration (NASA) through Remote Sensing Theory and Terrestrial Ecology programmes 80NSSC21K0568 and 80NSSC21K1702. M.C. also acknowledges support by a McIntire–Stennis grant (1027576) from the National Institute of Food and Agriculture (NIFA), United States Department of Agriculture (USDA). B.D. acknowledges support by sDiv, the Synthesis Centre of iDiv (DFG FZT 118, 202548816). J.X. was supported by the National Science Foundation (NSF) (Macrosystems Biology and NEON-Enabled Science programme: DEB-2017870). Y.R. was supported by the National Research Foundation of Korea (NRF-2019R1A2C2084626). The authors thank G. Badgley for fruitful discussions on vegetation indices and P. Köhler for the TROPOMI far-red daily SIF dataset.

Author contributions

Y.Z., M.C., D.H. and A.H. wrote the initial draft of the manuscript. All authors reviewed and edited the manuscript and made substantial contributions to the improvement of the manuscript.

Competing interests

The authors declare no competing interests.

Peer review information

Nature Reviews Earth & Environment thanks F. Tian, Z. Zhu and the other, anonymous, reviewer(s) for their contribution to the peer review of this work.

Publisher's note

Springer Nature remains neutral with regard to jurisdictional claims in published maps and institutional affiliations.

Supplementary information

The online version contains supplementary information available at <https://doi.org/10.1038/s43017-022-00298-5>.

© Springer Nature Limited 2022